PWA FR-4993
12 JUNE 1972

SUPPRESSION OF COMBUSTION OSCILLATIONS WITH MECHANICAL DAMPING DEVICES

FINAL REPORT

Prepared Under Contract NAS8-21310 for
George C. Marshall Space Flight Center
National Aeronautics and Space Administration
Huntsville, Alabama

Pratt & Whitney Aircraft DIVISION OF UNITED AIRCRAFT CORPORATION
FLORIDA RESEARCH AND DEVELOPMENT CENTER
BOX 2691, WEST PALM BEACH, FLORIDA 33402

Errata for Pratt & Whitney Aircraft Report PWA FR-4993, "Suppression of Combustion Oscillations with Mechanical Damping Devices, Final Report," dated 12 June 1972.

1. page 66, line 46 should read

   ENABC=P1**2*PRESS*SONIC*EPSLO*APARE/2./GAMA/SIG

2. page 67, line 32, should read

   ENABX=ENABO*RCOEF/EPSLO

PWA FR-4993
12 JUNE 1972

SUPPRESSION OF COMBUSTION OSCILLATIONS WITH MECHANICAL DAMPING DEVICES

FINAL REPORT

Prepared Under Contract NAS8-21310 for
George C. Marshall Space Flight Center
National Aeronautics and Space Administration
Huntsville, Alabama

Approved by: G. D. Garrison

G. D. Garrison
Program Manager

Pratt & Whitney Aircraft
DIVISION OF UNITED AIRCRAFT CORPORATION
FLORIDA RESEARCH AND DEVELOPMENT CENTER
BOX 2691, WEST PALM BEACH, FLORIDA 33402

FOREWORD

The report presents the results of work accomplished at Pratt & Whitney Aircraft, Florida Research and Development Center under Phase III of Contract NAS8-21310, sponsored by the NASA Marshall Space Flight Center. All work was performed during the period 27 June 1970 through 29 February 1972. Mr. R. H. Counts was the NASA Technical Monitor and Dr. Uno Ingard of the Massachusetts Institute of Technology served as technical consultant. The following personnel of Pratt & Whitney Aircraft contributed to the technical effort: P. L. Russell, J. W. Koenig, A. C. Schnell, and G. D. Garrison, who was the Program Manager.

CONTENTS

ILLUSTRATIONS

ILLUSTRATIONS (Continued)

ILLUSTRATIONS (Continued)

TABLES

NOMENCLATURE

Symbol	Description
A	Aperture Cross-Sectional Area
A_c	Cavity Cross-Sectional Area
A_{opt}	Aperture Area Producing Peak Absorption
B	Constant = KC_f^{-2}
b	Spacing Distance for Array
C_f	Aperture Flow Coefficient (Discharge Coefficient)
c	Aperture Gas Sonic Velocity
d	Aperture Diameter
f	Frequency
I	Incident Energy Intensity
I_a	Absorbed Energy Intensity
K	Resistance Coefficient (0.37 for Circular Apertures)
k	Wave Number
L	Cavity Backing Depth
ℓ	Effective Aperture Length
L_e	Effective Length of Quarter Wave Cavity
M	Mach Number
m	Dimensionless Particle Velocity Parameter = Bu/c
P	Static Pressure
p_i	Incident Sound Pressure
Q	Quality Factor
R	Dissipation Resistance
R_r	Radiation Resistance
T_a	Aperture Gas Temperature (Rankine)
T_c	Combustion Gas Temperature (Rankine)
t	Aperture Length
u	Peak Particle Velocity
V	Volume of Resonator Cavity
W	Power Absorbed
X	Reactance
Z	Total Impedance
α	Absorption Coefficient
β	Nonarray Specific Resistance Ratio, Dissipation to Radiation
γ	Ratio of Specific Heats

NOMENCLATURE (Continued)

Symbol	Description
δ	Effective Length Correction Factor, Defined by $\ell = t + \delta d$
ϵ	Resonator Coefficient
ϵ'	Absorbing Cross Section = W/I
ζ	Frequency Ratio = f/f_o
θ	Array Specific Resistance Ratio
θ_r	Dimensionless Radiation Resistance = $R_r/\rho c$
λ	Wavelength
μ	Inertance
ρ	Aperture Gas Density
σ	Facing Open Area Ratio for Array
σ_c	Cavity Open Area Ratio = A/A_c
Υ	Gas Constant
ω	Angular Frequency

General Subscripts

Symbol	Description
max	Maximum
o	Denotes Conditions at Resonance
p	With Flow Past Aperture
T	With Flow Through Aperture

SECTION I
PROGRAM SUMMARY

A. BACKGROUND

Past efforts at Pratt & Whitney Aircraft on absorbing liners have been limited to theoretical analysis and experimental evaluation of designs consisting of arrays of Helmholtz-type resonators. These devices are efficient combustion instability suppressors primarily because, when properly designed, they can absorb a large percentage, if not all, of the pressure wave energy acting on the surface of the liner. An array covering a significant portion of the combustion chamber surface is desirable to ensure stable combustion. However, in many instances (particularly cases of existing thrust chambers in which attempts to uprate performance are thwarted by the appearance of combustion instability), surface areas are limited and only a few resonators can be installed. Under this circumstance, the resonator array theory is not valid; in fact, both the absorption coefficient and the open area ratio used in the theory can only be arbitrarily defined.

B. OBJECTIVE AND APPROACH

For acoustic energy absorbers other than arrays of resonators, such as single Helmholtz resonators, slots, and quarter-wave tubes, a design analysis based on total energy absorption was believed to be a valid approach, but no theory was available for use in the nonlinear acoustic regime, where rocket chamber acoustic devices must operate. Effort under Phase III of the program was therefore devoted to the development and verification, using cold-flow acoustic devices, of such a design theory for nonarray absorbing devices. Other cold-flow acoustic experiments were conducted to investigate the dimensional limitations of acoustic suppression devices, including resonators, slots, and quarter-wave tubes. The acoustic data were obtained using existing impedance measuring devices at Pratt & Whitney Aircraft and from a new acoustic reverberation system that was procured specifically for use under the program.

C. CONCLUSIONS AND RECOMMENDATIONS

It is concluded that individual acoustical devices can be designed for maximum acoustic energy absorption using the theory developed herein. Furthermore, the theory may be used to design multiple elements with arbitrary spacing between the apertures, but if the spacing is closer than a certain limiting value, the elements must be treated as an array. However, at this limit, no discontinuity

in the theory exists; the nonarray dependent variable, the resonator coefficient, is equal to the array dependent variable - the absorption coefficient.

For the design of absorbing devices the following values of the resistance coefficient, K, are recommended:

Resonators	0.37
Quarter-wave tubes	0.75
Quarter-wave slots	0.53

Whenever possible, it is recommended that resonators be used in lieu of quarter-wave length slots or tubes because resonators inherently dissipate more acoustic energy per cycle, and they can be designed for wide-band absorption to allow for inaccuracies in predicting the frequencies of resonance and the frequencies of the oscillations to be damped.

Quarter-wave length absorbing devices have fundamental frequencies that correspond to lengths greater than the actual. The effective length and the actual fundamental frequency can be approximated using a simple technique discussed herein.

The number of apertures used to produce a resonator of given total open area with a common, unpartitioned cavity is immaterial unless the device is cavity-volume-limited. If so, highest absorption will be obtained with the fewest number of apertures.

The apertures of absorbing devices may be placed adjacent to or in the corners formed by injector faces, baffles, etc., with no detriment to the acoustical characteristics of the device. In fact, the power absorption will be slightly improved in a predictable manner.

It is recommended that single resonators be designed so that the ratio of the aperture diameter to the product of the quarter-wave length and cavity backing depth is less than one. Otherwise, the absorbing characteristics of the actual device can be less than theory predicts.

From experiments with resonators having long apertures with respect to the quarter-wave length, it was shown that absorption at the harmonic frequencies can be as high as that of the fundamental. An analytical technique for predicting the resonance frequencies and the absorption at any frequency was developed and included in the nonarray device design computer program. The program, which can be used to design both resonators and acoustic cavities, is included herein as Appendix C.

SECTION II
DERIVATION OF THEORY

For the design of nonarray absorbing devices for use in rocket thrust chambers, a comprehensive theory is required to relate the acoustical characteristics to the physical dimensions of the device. Other factors that must be included in the theory are the properties of the media in which the device operates and the effects of media flow, if present, on the acoustics of the system. A great number of publications dealing with nonarray acoustic elements for architectural applications (especially single Helmholtz resonators) have been published. However, none has presented a theory suitable for rocket application, primarily because the sound pressure amplitudes and flow fields peculiar to rocket motors are rather unique.

A. BASIC DERIVATIONS

For a resonant acoustic device, e.g., a single Helmholtz-type resonator, with dimensions small with respect to wavelength, mounted in an infinite wall subjected to sound waves of normal incidence, the total specific impedance is, by definition, the following function of the complex ratio of incident pressure, p_i, to particle velocity, u:

$$Z = 2p_i/u \tag{1}$$

If ρ and c are the media density and sonic velocity, respectively, the incident energy intensity is

$$I = p_i^2/2\rho c \tag{2}$$

and the power absorbed by the device is

$$W = u^2RA/2 \tag{3}$$

where R is the dissipation resistance and A is the aperture area. The absorbing cross section, ϵ', is, by definition (Reference 1)

$$\epsilon' = W/I \tag{4}$$

which, by using the preceding equations, can be expressed as

$$\epsilon' = 4\rho cAR|Z|^{-2} \tag{5}$$

As shown in Reference 1 the maximum absorbing cross section for a particular frequency of wavelength λ is

$$\epsilon'_{max} = \lambda^2/2\pi \tag{6}$$

If a resonator coefficient is defined as $\epsilon = \epsilon'/\epsilon'_{max}$, equations (5) and (6) may be used to produce

$$\epsilon = 8\pi\rho c\, AR\, (\lambda|Z|)^{-2} \tag{7}$$

For a single resonator in an infinite wall the radiation resistance, Reference 1, is

$$R_r = 2\pi\rho c A\lambda^{-2} \tag{8}$$

which, when substituted in equation (7) gives

$$\epsilon = 4\, R_r R\, |Z|^{-2} \tag{9}$$

The significance of ϵ, the resonator coefficient, is similar to that of the absorption coefficient used for resonator arrays. It is both a measure of the energy absorbing characteristics and the efficiency of a resonator. The resonator coefficient can only vary between 0 and unity; values near zero mean that essentially all of the acoustic energy incident in the vicinity of the resonator is being reflected (or reradiated) and little absorbed. Values of ϵ near unity mean that the resonator is absorbing as much of the incident energy as can be absorbed. Values of ϵ less than unity indicate that at least theoretically it is possible to select a different resonator configuration that will absorb more acoustic energy.

The total specific impedance of an individual resonator is

$$Z = R + R_r - iX \tag{10}$$

which can be used to put equation (9) in the form

$$\epsilon = \frac{4\beta}{(\beta + 1)^2 + (X/R_r)^2} \tag{11}$$

where $\beta = R/R_r$. From previous work, Reference 2, it is known that the dissipation resistance can be computed using

$$R = K\rho u C_f^{-2} \tag{12}$$

where K is the resistance coefficient (0.37 for circular apertures), and C_f is the aperture discharge coefficient.

For a Helmholtz-type resonator the reactance for use in equation (11) is found from

$$X = -(A/A_c)\rho c \cot(\omega L/c) + \omega\rho\ell \tag{13}$$

where ω is the angular frequency, A_c is the cavity cross-sectional area, L is the cavity backing depth, and ℓ is the effective aperture length. For high sound levels a good approximation for ℓ is known from Reference 1 to be

$$\ell = t + \delta d$$

where

$$\delta = 0.85\ (1 - 0.71\sqrt{\sigma_c}). \tag{14}$$

In the above equations t is the aperture length, d is the aperture diameter, and σ_c, the cavity open area ratio is defined as

$$\sigma_c = A/A_c.$$

B. MULTIPLE ELEMENTS

The nonarray acoustic theory will now be extended for application to multiple elements with arbitrary spacing between the apertures. It will be shown that if the spacing is closer than a certain limiting value (which is a function of frequency) the elements can be treated as an array. Furthermore, at this limit no discontinuity in the theory exists; the nonarray dependent variable, the resonator coefficient, is equal to the array dependent variable, the absorption coefficient.

Let the absorbing device consist of an array of resonators with circular apertures of diameter d spaced a distance b apart in a square pattern. Although the facing (or incident) area per resonator is always b^2, the maximum absorbing cross section, $\lambda^2/2\pi$, can only be obtained if the facing area for each resonator in the array is a least equal to $\lambda^2/2\pi$; this means the limit in the single resonator theory occurs when

$$b^2 = \lambda^2/2\pi \tag{15}$$

or

$$b \simeq 0.4\lambda \tag{16}$$

If $b \leq 0.4\lambda$ the maximum absorbing cross section is simply b^2, and the resonator coefficient by definition becomes

$$\epsilon = \epsilon' b^{-2} = W/Ib^2 \tag{17}$$

where W is still as defined by equation (3). The quantity W/b^2 in the above equation is actually the absorbed energy intensity, I_a, which causes equation (17) to become by definition the absorption coefficient, α of the array; i.e.,

$$\epsilon = \frac{W}{Ib^2} = \frac{I_a}{I} = \alpha \tag{18}$$

For the special case $b = 0.4\lambda$, substituting equation (15) in equation (8) gives the expression for the radiation resistance for arrays,

$$R_r = \rho c \sigma \tag{19}$$

where σ is the facing open area ratio, A/b^2. Equation (19) is also correct for all values of $b < 0.4\lambda$.

To determine the absorption coefficient, equations (12) and (13) are used for R and X and the coefficient is computed from

$$\alpha = \frac{4\theta}{(\theta + 1)^2 + (X/\sigma\rho c)^2} \tag{20}$$

where θ, the specific resistance ratio, is defined as $R/\rho c \sigma$.

Note that for $b = 0.4\lambda$ either equation (11) or (20) can be used to compute the dependent variable because

$$R_r = 2\pi\rho c A \lambda^{-2} = \rho c \sigma \tag{21}$$

which means that for this case $\epsilon = \alpha$, and that no discontinuity in the theory exists.

C. OPTIMUM CONDITIONS

It is known for arrays that the condition $\alpha = 1$ maximizes the power absorbed. Proof that a similar condition exists for individual elements follows:

Using equation (12), the power dissipated, equation (3) may be written as

$$W = 1/2 A \rho c^3 B^{-2} m^3 \tag{22}$$

where B and m are defined as

$$B = KC_f^{-2} \tag{23}$$

and

$$m = Bu/c \tag{24}$$

The relationship between particle velocity, incident sound pressure, and impedance at resonance is

$$u_o = 2p_i/(R_r + R)_o \tag{25}$$

which, by using the above definitions can be written as

$$m_o = \left(\frac{2p_i B}{\rho c^2}\right)\left(\frac{R_r}{\rho c} + m_o\right)^{-1} \tag{26}$$

If P is the static pressure, the perfect gas equations for density and sonic velocity can be used to obtain

$$\rho c^2 = \gamma P \tag{27}$$

where γ is the ratio of specific heats.

By letting $\theta_r = R_r/\rho c$, using equation (27) and rearranging, equation (7) becomes

$$m_o^2 + \theta_r m_o = \frac{2p_i B}{\gamma P} \tag{28}$$

which has for a solution

$$m_o = -\frac{\theta_r}{2} + \sqrt{\left(\frac{\theta_r}{2}\right)^2 + \frac{2p_i B}{\gamma P}} \tag{29}$$

It may be shown that for this case,

$$\theta_r = k^2 A/2\pi \tag{30}$$

thus, by substituting equations (29) and (30), equation (22) becomes

$$W_o = 1/2\rho c^3 B^{-2} A\left[\sqrt{\left(\frac{k^2 A}{4\pi}\right)^2 + \frac{2p_i B}{\gamma P}} - \frac{k^2 A}{4\pi}\right]^3 \tag{31}$$

This equation gives the power dissipated at resonance by a nonarray absorber as a function of aperture area and incident sound pressure. For design purposes a more useful expression would be one from which the optimum aperture area could be determined. Such an expression is obtained by equating with zero the first derivative of equation (31) with respect to A. The resulting equation,

$$A_{opt} = \frac{2\pi}{k^2}\sqrt{\frac{p_i B}{\gamma P}} \tag{32}$$

which may also be written

$$A_{opt} = \frac{\lambda^2}{2\pi}\sqrt{\frac{p_i B}{\gamma P}} \tag{33}$$

shows that for a given media the aperture area that produces maximum power dissipation is a function of both the frequency and amplitude of the incident wave.

Substituting the above equation back into equation (31) gives the expression for the maximum power that can be absorbed, i.e.,

$$W_{max} = \frac{(\lambda p_i)^2}{4\pi\rho c} \tag{34}$$

Using equations (4) and (6) with the definition of the resonator coefficient, $\epsilon = \epsilon'/\epsilon'_{max}$, produces

$$\epsilon = \left(\frac{W}{I}\right)\frac{2\pi}{\lambda^2} \tag{35}$$

which shows that for a given sound pressure and frequency ϵ will be maximized when $W = W_{max}$. The proof is completed by substituting equations (2) and (34) into equation (35) which results in

$$\epsilon_{W_{max}} = 1.0 \tag{36}$$

Inspection of equation (11) shows that $\epsilon = 1$ can only result if $X = O$ and $\beta = 1$ i.e., if $R = R_r$ at resonance.

D. OFF-RESONANCE THEORY

To obtain an expression for the off-resonance behavior of the resonator coefficient the quality factor Q, which is defined (Reference 4) as

$$Q = \omega_o \mu/(R+R_r)_o \tag{37}$$

is used; this parameter is a measure of the sharpness of resonance (or bandwidth absorbing characteristics) of a driven resonator. For a Helmholtz-type resonator the inertance is

$$\mu = \rho \ell \tag{38}$$

thus, equation (37) can be written as

$$Q = \omega_o \rho\ell/(R+R_r)_o \tag{39}$$

or, using $\beta = R/R_r$ and equation (8), as

$$Q = \frac{\lambda_o \ell}{A(\beta_o + 1)} \tag{40}$$

It is reasonable to assume that at frequencies near resonance the resistance is constant; then the total impedance can be written as

$$Z = (R+R_r)_o \left[1-iQ(\zeta-1/\zeta)\right] \tag{41}$$

where ζ is the frequency ratio, f/f_o.

Substituting equation (41) into equation (9) produces an expression for the resonator coefficient as a function of frequency

$$\epsilon = \frac{4\beta_o}{(\beta_o+1)^2} \quad \frac{1}{1 + Q^2 \ (\zeta-1/\zeta)^2} \tag{42}$$

Where required in any of the above equations, the frequency of resonance, f_o, is obtained by solving equation (13) for X = O, or, if $L << \lambda$ computed from

$$f_o = \frac{c}{2\pi} \left[\frac{A}{V\ell}\right]^{1/2} \tag{43}$$

where V is the volume of the resonator cavity.

E. PAST-FLOW THEORY

Rocket chamber acoustic devices must usually operate with a net flow of combustion gases past their apertures. It has long been known that the past-flow causes the acoustic resistance of the absorber to be greater than if there were no flow and causes resonance to occur at a slightly different frequency. Attempts to quantitatively determine the flow effects have been made (References 2, 5, and 6); however, results from the different experiments were inconsistent and, in addition, because of the limited range of velocities, had to be extrapolated for most rocket chamber applications. Recently, (Reference 7) both cold flow experiments and firings of a dynamically unstable rocket motor containing small absorbers were conducted and the flow effects were measured with Mach numbers up to 0.73. It was found that

1. Effective aperture length with flow past the apertures is best described by

$$\ell_p = t + 0.375 \ [0.85d \ (1-0.7\sqrt{\sigma_c})] \tag{44}$$

where σ_c is the cavity open area ratio, A/A_c. This value of ℓ_p should be used instead of that from equation (14) to compute the frequency of resonance, reactance, and other design parameters.

2. Acoustic resistance, if

$$\frac{M_p}{(u/c)} \left(\frac{T_c}{T_a} \right)^2 > 1.5 \tag{45}$$

where M_p is the Mach number of the past-flow and T_c and T_a are the chamber and aperture gas temperatures (°R), respectively, should be computed from

$$R_p = \frac{1}{3} \quad B\rho c \; M_p \; (T_c/T_a)^2 + \frac{1}{2} \quad B\rho u \tag{46}$$

If the above inequality (45) is <u>not</u> satisfied the effects of flow can be ignored.

An expression for the optimum area with high velocity past-flow can be obtained by using the required conditions for $\epsilon = 1$, i.e., $R_p = R_r$, and $X = O$. For this case

$$u_o = \frac{2p_i}{(R_p + R_r)_o} = \frac{p_i}{(R_r)_o} \tag{47}$$

Setting equation (46) equal to equation (8), substituting equation (47), and rearranging produces

$$\left(A_{opt}\right)_p = \frac{2\pi}{k_o^2} \left[(BM_p/6) \; (T_c/T_a)^2 + \sqrt{(BM_p/6)^2 \; (T_c/T_a)^4 + \frac{Bp_i}{2\gamma P}} \right] \tag{48}$$

For the special case

$$\frac{M_p}{(u/c)} \left(\frac{T_c}{T_a} \right)^2 = 1.5 \tag{49}$$

either equation (12) or (46) can be used to determine resistance and either equation (32) or (48) for the optimum area.

F. THROUGH-FLOW THEORY

If there is net flow of Mach number M_T through the absorber aperture such that $M_T > u/2c$, then the resistance is (Reference 2)

$$R_T = \frac{\rho M_T}{C_f^3} \tag{50}$$

and the optimum area becomes

$$\left(A_{opt}\right)_T = \frac{\lambda^2}{2\pi} \frac{M_T}{C_f^3} \tag{51}$$

For high incident pressures (160 db* and greater) the effects of through-flow on reactance (and therefore on effective length and resonance) were found to be negligible (Reference 2). Furthermore, if $M_T < u/2$ the effect of through flow on resistance can be ignored.

In some applications there will be net flows both through and past the absorber aperture; however, as shown in Reference 8, the absorber can be treated as if only through-flow were present.

G. LIMITING CONDITION

All of the above analysis is valid only if the viscous resistance of the absorbing device is small in comparison to the nonlinear resistance. From previous experiments with circular apertures (Reference 2) it is known that this condition is fulfilled when

$$p_i/P \geq 666\gamma \, (c \; C_f)^{-2} \tag{52}$$

Rocket chamber acoustic devices are typically designed for dynamic pressure amplitudes of at least 1% of the static combustion pressure, i.e., $p_i/P = 0.01$, which is well above the limiting value of equation (52).

H. NONARRAY DEVICE COMPUTER PROGRAM

A FORTRAN IV design computer program is included herein as Appendix C. For a device of given dimensions the impedance, resonator coefficient, and other acoustical parameters are computed at resonance and, if desired, over a range of

*In this report all sound pressures expressed in decibels (db) are based on a reference pressure of 0.0002 microbar.

frequencies and incident-to-static pressure ratios. The theory used in the program is identical to the above, with one exception: it was not necessary to assume the resistance was constant for the off-resonance computations because an iterative solution of the impedance equation (1) was used to determine the particle velocity, i.e., u is computed by solving

$$u = 2p_i/(R + R_r - i X). \tag{53}$$

SECTION III
EXPERIMENTAL PROGRAM

A. REVERBERATION SYSTEM

A reverberation system was fabricated and used to provide cold-flow acoustic data for verification and improvement of the theory for the design of nonarray absorbing elements. The system as illustrated in figure 1 consists of a chamber, embedded inside a gravel-filled bunker, driven by two electropneumatic transducers mounted on exponential horns. The internal volume of the reverberation system, including the horns, is approximately 35 ft^3. The chamber (figure 2) is pentagonal in cross-section with walls 2 ft wide and an overall chamber length of 4-1/2 ft; one endwall is tilted 10 deg off-vertical to prevent the formation of a uniform longitudinal mode. Gaseous nitrogen used to drive the electropneumatic transducers exhausts through four 1-in. pipes on which low-pass filters are mounted to reduce the amount of sound energy escaping from the chamber. All instrumentation leads are introduced to the inside of the chamber through a 2-in. pipe mounted on the sidewall of the chamber. This pipe was plugged at the chamber end so that it would not affect the results of reverberation tests. A 1-1/2-in. pipe was provided to introduce a secondary gas flow for tests requiring a flow of gas past or through the acoustic element being tested. Large plates mounted on the side and endwalls of the chamber serve as compactors to help settle the gravel tightly around the chamber walls, thus reducing vibration and loss of sound energy from inside the chamber.

Electronic equipment used in the reverberation measurements is shown in the block diagram presented as figure 3. A General Radio random-noise generator was used to provide a noise signal with a Gaussian amplitude distribution, and a Technical Products wave analyzer was used to select a narrow band of the noise (250 Hz) for use as a signal to drive the reverberation chamber. The narrow-band noise signal was then amplified and introduced into the reverberation chamber through two Ling electropneumatic transducers. Four Bruel and Kjaer 1/4-in. microphones were suspended inside the chamber with the outputs connected to a four-way selector box. Each microphone signal could then be individually selected and passed through a General Radio wave analyzer; the filtered signal was recorded on a Bruel and Kjaer graphic recorder in the form of decibels versus time. Two microphone signals were connected to the phase-measuring

system so that pressure-phase data could also be obtained. A discussion of reverberation techniques that were used with the apparatus appears in Appendix A.

1. Preliminary Experiments

Cold flow tests were conducted to evaluate the system response, i.e., reverberation decay times, with different types of test signals used to generate the sound field within the chamber. A random noise signal with a uniform spectrum density (white noise) in the frequency range 20 Hz to 20 kHz and having a Gaussian magnitude distribution was used in the first set of tests.

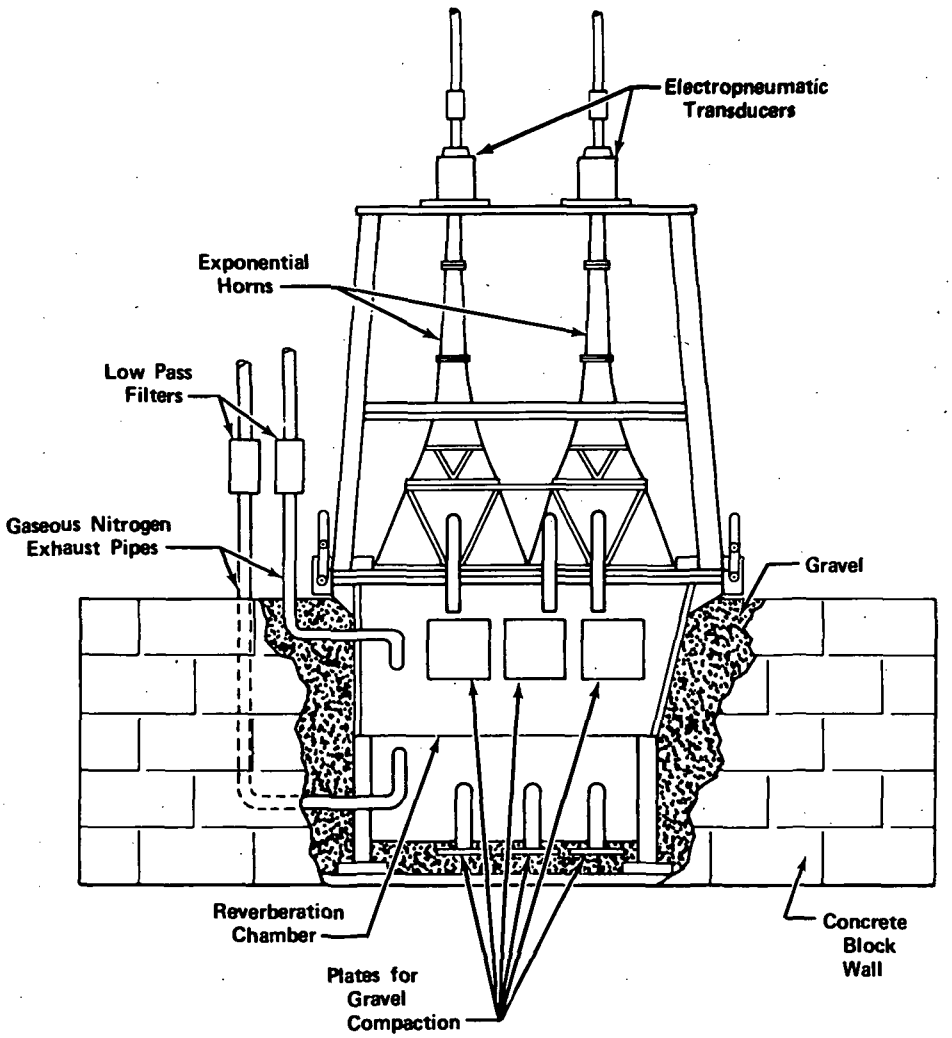

Figure 1. Reverberation System FD 44696

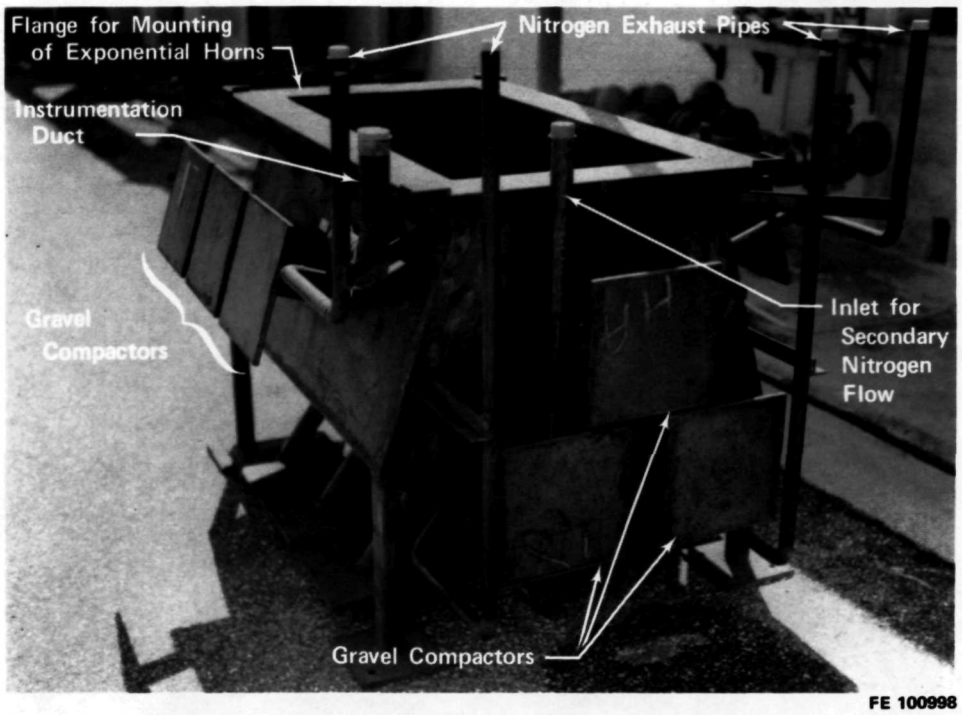

Figure 2. Reverberation Chamber FD 44697

Maximum sound pressure levels (SPL) of less than 135 db were measured at selected frequencies in the range of 500 Hz to 2000 Hz. By turning off the random noise signal it was found that the background noise resulting from the gaseous nitrogen flow through the pneumatic sound drivers was fluctuating with SPL's between 100 and 110 db. The difference between the test signal and the background noise in each test was less than 25 db, which resulted in short fluctuating decay curves from which accurate decay times were difficult to measure.

A pure tone sinusoidal test signal was used in a second set of tests in an attempt to produce higher sound pressure inside the chamber. It was found that sound pressures greater than 170 db could be generated at frequencies up to 1000 Hz with levels greater than 150 db up to 2000 Hz. With pressure amplitudes of this magnitude it was possible to record decay rates over a 30 db range completely within the nonlinear sound pressure regime. The disadvantage of using a pure tone signal is that organized modes were established inside the chamber resulting in a spatially nonuniform sound field with sound pressure variations of up to ±12 db.

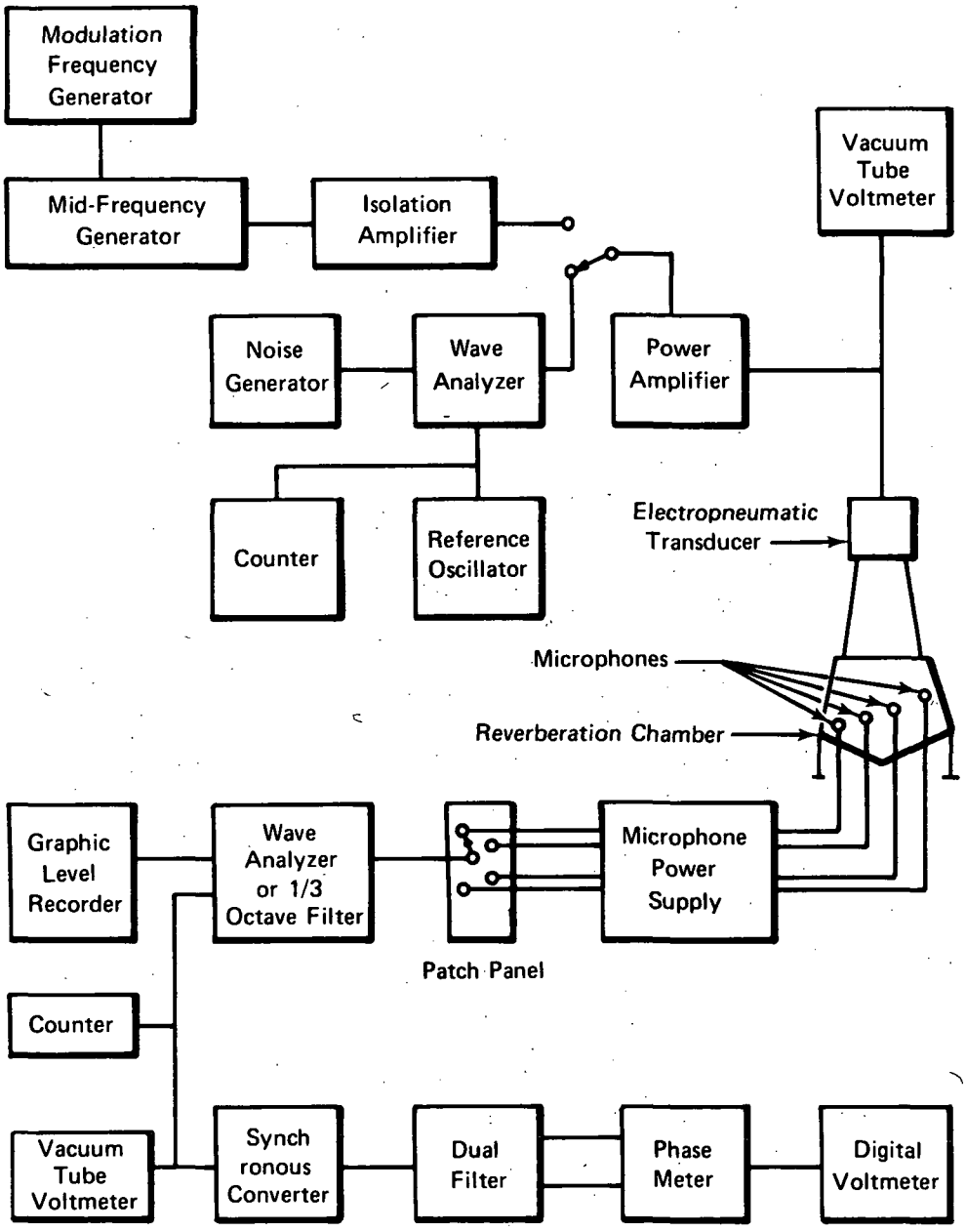

Figure 3. Block Diagram of Electronic Equipment Used in Reverberation System FD 61300

Use of the Sabine reverberation method to measure the absorption of an acoustic specimen requires that the distribution of sound energy be uniform inside the chamber. To improve the distribution of sound energy, a modulated frequency (warble tone) test signal was used in a series of additional cold flow tests. The modulated frequency signal was generated by using a Wavetek

sweep/trigger Voltage Controlled Generator (VCG). The modulated frequency signal is generated by selecting a mid-frequency value for the primary generator output and simultaneously applying a second modulation frequency parallel to the primary generator output. The amplitude of the modulation frequency signal controls the upper and lower frequency limits between which the primary generator oscillates.

Analysis of tests made with the frequency modulated signal showed that a significant improvement in sound distribution was achieved; the fluctuations were reduced to a level of ±2 db. It was decided that this energy distribution was satisfactory, and that cold flow tests could be conducted to evaluate the accuracy of the reverberation system by measuring the absorption coefficient of liner arrays having known acoustical properties.

2. Evaluation Experiments

The evaluation tests were conducted using a modulated signal with a mid-frequency of 1000 Hz and a modulation frequency of 10 Hz with a bandwidth having the same peak width as the one-third octave filter (figure 4) used to condition the output signal from the microphones mounted inside the chamber. In each of three series of tests reverberation decay curves were obtained using twelve different microphone positions inside the chamber.

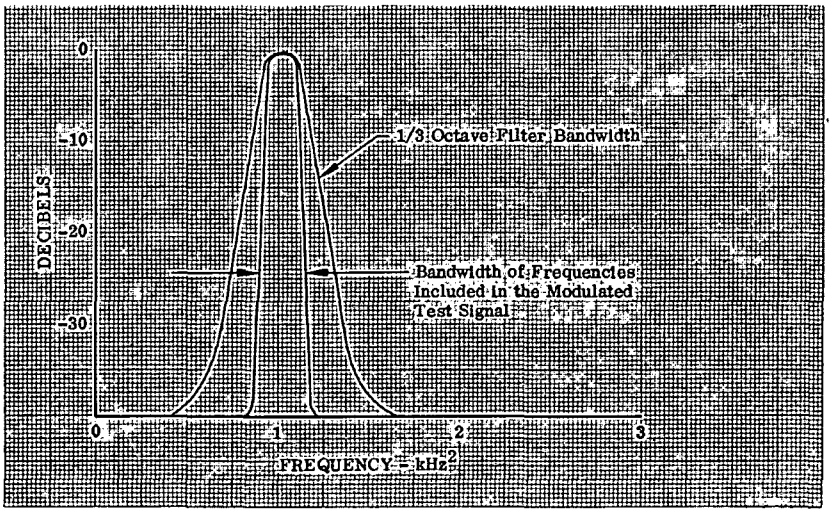

Figure 4. Comparison of Test Signal Power Spectrum and 1/3 Octave Filter Bandwidth DF 90636

The first experiments were made without a liner inside the chamber to determine the average absorption of the chamber walls and to obtain the baseline decay rate; a total of 150 decay curves were recorded. In the second series of tests a liner with known absorption characteristics was mounted flat on the sidewall of the chamber. The liner was a full array having an incident surface area of 144 sq in. with an open area ratio of 5.5%, aperture diameter of 0.093 in., liner faceplate thickness of 0.1 in., and a backing cavity depth of 1.5 in. Theoretically, the liner was tuned for resonance at 1000 Hz, which would produce approximately 1.0 Sabine of absorption within the modulation frequency bandwidth. (See figure 5.) A third series of experiments was conducted to determine if small absorption values (approximately 0.5 Sabine) could be measured. In these tests the same liner faceplate was used but the cavity backing distance was changed to 0.88 in. increasing the resonant frequency to 1350 Hz; as shown in figure 5 the average theoretical absorption in the 1000 Hz modulation frequency bandwidth was reduced to approximately 0.6 Sabine. A total of 132 decay curves were recorded.

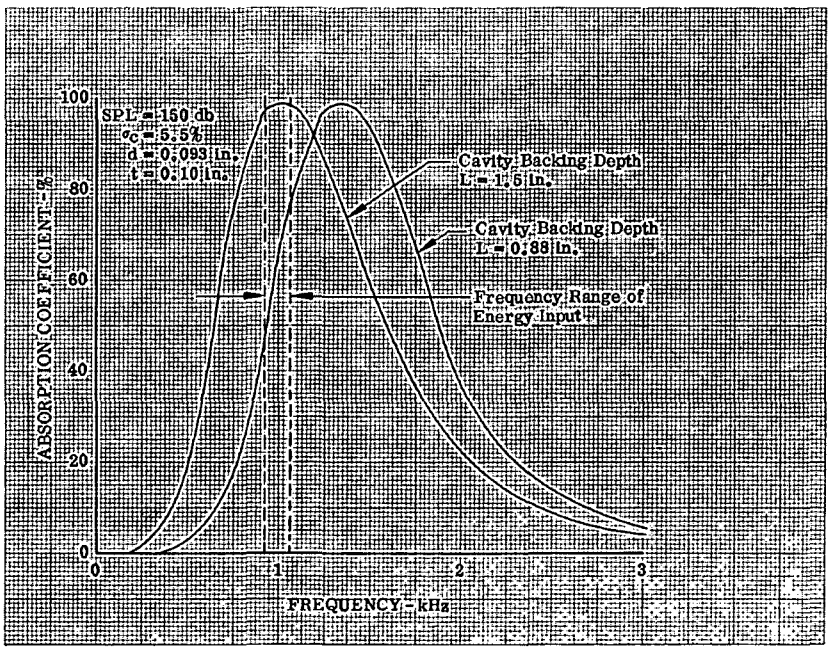

Figure 5. Theoretical Absorption Characteristics of Liners Used in Evaluation Test Series DF 90637

Analysis of the data was based on the proposal of Sabine that the absorption coefficient of an acoustic specimen be calculated from the equation

$$\alpha = \frac{0.92V}{Sc}\,(D'-D) \qquad (54)$$

where:

V_c = the volume of the reverberation chamber

S = the surface area of the test section

D' = the decay rate and

D = the baseline decay rate.

The decay times for a 20 db drop were measured from the reverberation decay curves for all three series of tests and then used to determine the decay rates. Typical decay curves are shown in figure 6 and a summary of the test results is presented in table I.

Table I. Reverberation Test Results

Type of Test	Number of Data Points	Avg 20-db Decay Time, sec	Avg Measured Absorption, %	Theoretical Absorption, %	Experimental Error, %
Baseline	150	0.28	-	-	-
High Absorption	120	0.20	87	99	12
Low Absorption	132	0.23	51	62	18

For the resonant (high absorption) tests the agreement between theory and experiment is probably as good as can be expected for this type of experiment. The more significant difference in absorption between theory and experiment in the off-resonance (low absorption) tests is believed to be the result of the rapid change in absorption with frequency over the range of input frequencies (figure 5), thereby permitting a small error in the measured decay rate to produce a large uncertainty in absorption. From the above results it was concluded that the reverberation method is the most accurate when the liner elements are tested at resonance, giving maximum absorption and a minimum change of absorption with frequency over the band of frequencies covered by the modulated test signal. However, the acoustic devices to be used to develop the nonarray theory would have have to be tested not only at resonance, but over a wide range of frequencies. Because use of the reverberation method alone would introduce considerable experimental uncertainty, it was decided to instrument all test sections for pressure-phase measurements and use the equations of Appendix B for determining impedance. The reverberation chamber, driven with a sinusoidal signal would be used as a source of high-amplitude incident sound waves.

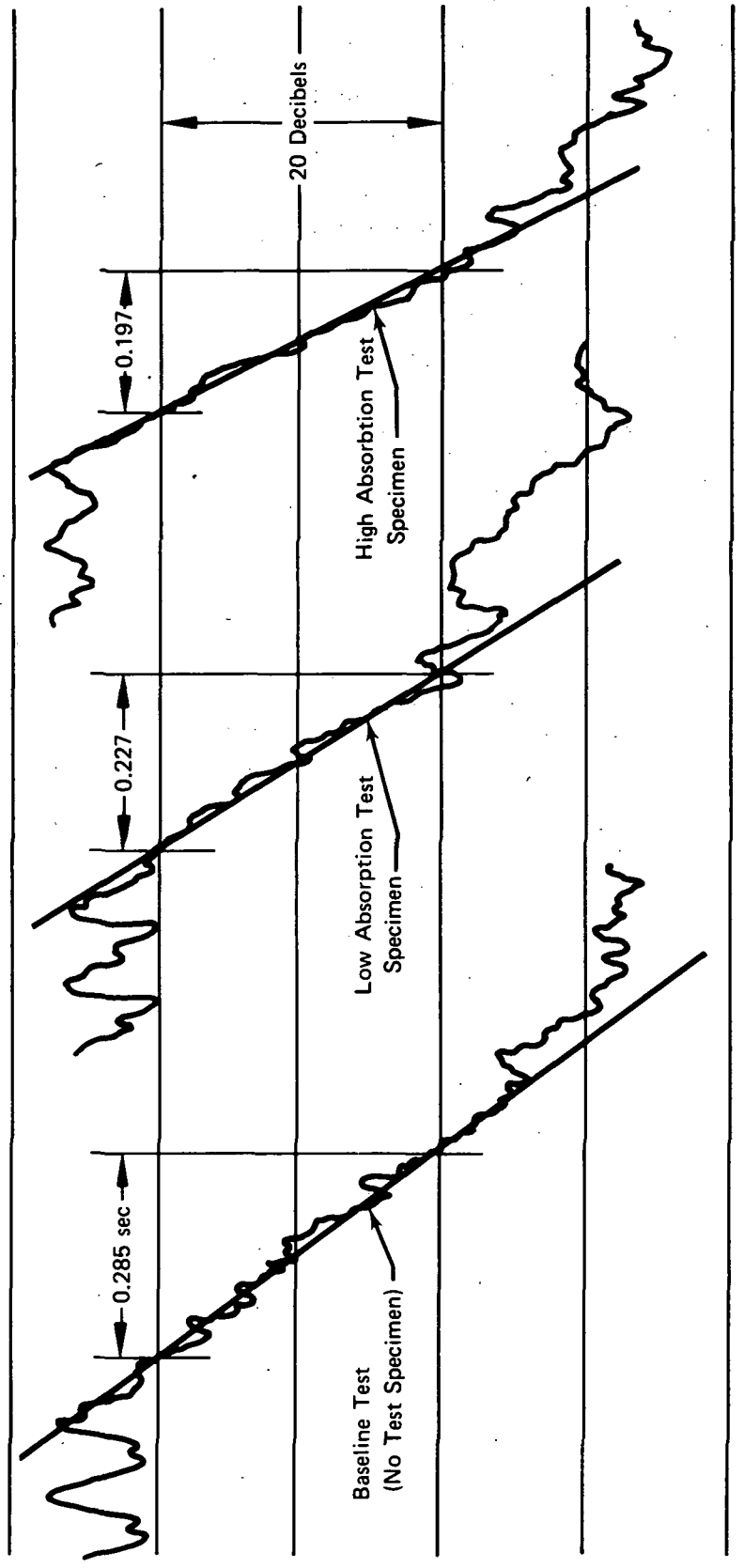

FD 61301

Figure 6. Typical Reverberation Decay Curves at 1000 Hz

B. VERIFICATION EXPERIMENTS

Acoustic experiments were performed to obtain data for verification and/or improvement of the nonarray design theory. The reverberation chamber was used as a sound source and the pressure-phase technique was used to obtain the impedance data. The nonarray devices used in the experiments were single aperture resonators (figure 7) fabricated from sections of pipe and a steel plate. The backing cavity depth could be adjusted from 0 to 7 in. by moving the piston-type rear wall; an O-ring was used to acoustically seal the resonator cavity volume and to hold the piston securely in position while testing. The resonator was located in the center of 1-foot square plate to simulate a resonator mounted in a wall.

Four series of resonator tests were conducted. In the first series of tests the resonator had an aperture diameter of 0.75 in. and a backing cavity depth of 0.78 in. producing a 750 Hz theoretical frequency of resonance. The resonator was placed on the bottom of the reverberation chamber and a pure sinusoidal signal was used to generate the sound field inside the chamber. The actual frequency of resonance was determined by varying the frequency of the test signal until a phase shift of 90-deg was measured between the facing pressure and the cavity rear wall pressure. After resonance was determined pressure-phase data were obtained at that frequency and then at frequencies both above and below resonance. Data were obtained over the range of frequencies at sound pressure levels of 135, 140, 150, and 160 db.

The above procedure was repeated for each series of tests, but before each series the aperture diameter was increased by remachining the original aperture. Before the fifth series of tests, the individual resonator was transformed into a quarter-wave tube by increasing the aperture diameter to the cavity diameter and setting the backing depth equal 4.64 in., the theoretical quarter-wave length for a frequency of 730 Hz. In table II is a summary of the resonator dimensions for each of the experiments.

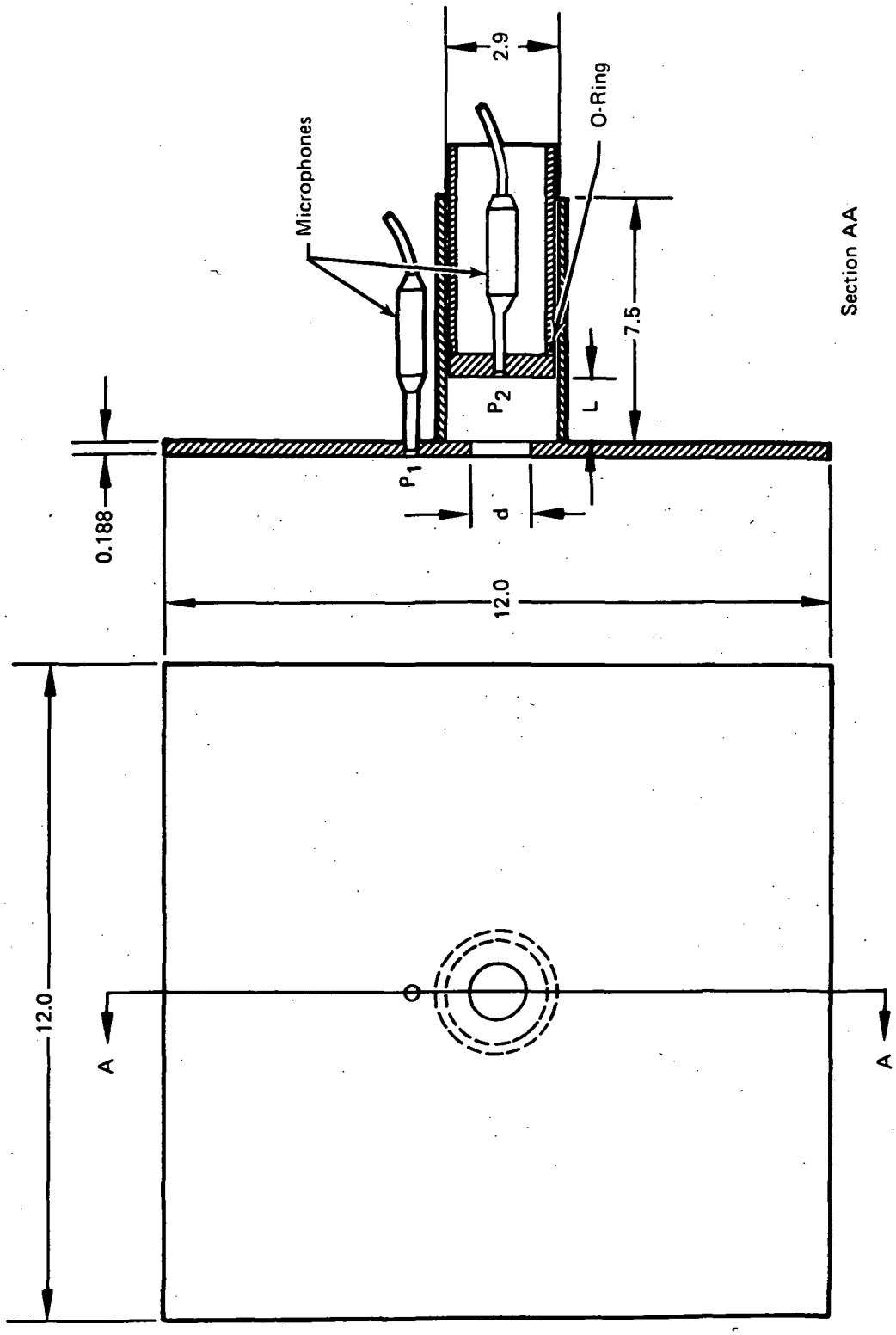

FD 61302

Figure 7. Typical Single Aperture Resonator Used in Nonarray Cold Flow Tests

Table II. Dimensions of Acoustic Devices Used in First Series of Verification Tests

Test Series	Aperture Diameter, in.	Backing Cavity Depth, in.	Theoretical Resonant Frequency, Hz
1	0.75	0.78	750
2	1.0	1.16	790
3	1.5	2.22	675
4	2.5	3.53	760
5	2.9	4.64	730

The acoustic resistance and reactance data were analyzed by computing the resistance coefficient, K, from

$$K = RC_f^2/\rho u \tag{55}$$

and the effective aperture length coefficient, δ, from

$$\delta = (\ell - t)/d \tag{56}$$

and comparing the results to the existing theory.

For the resonators, as expected, the resistance coefficient was, on the average, the same as that of arrays, i.e., 0.37; however, the quarter-wave tube was found to have a K value twice that of the array. This is because in a quarter-wave tube that is subjected to high incident sound fields a jet can form only during that part of the cycle in which there is flow out of the cavity whereas in a resonator a jet can form during both parts of the cycle. At high sound levels most of the acoustic energy is dissipated in the jet; thus, the tube will have approximately one-half the energy dissipation and, because dissipation and resistance are inversely proportional, twice the resistance of a resonator of the same aperture size.

The experimentally determined effective aperture lengths were used in equation (56) to compute δ; an average value of 0.66 was obtained which is in agreement with theory, equation (14). The averged value of δ, and a K value of 0.37, was then used with the theory of Section II to compute resonator coefficients for the resonators. Two types of off-resonant calculations were made; the first by assuming the resistance was a constant equal to the resonant value, and the other, as explained in Section II, by solving the impedance

equation using an iterative procedure. Typical results are shown in figure 8. In the vicinity of resonance, either type of calculation agrees with the experiment; however, at frequencies far from resonance the iterative procedure, as expected, produced better results.

A K value of 0.75 and the iterative procedure was used to compute resonator coefficients for comparison with the quarter-wave tube data. As shown in figure 9 the agreement between theory and experiment was good.

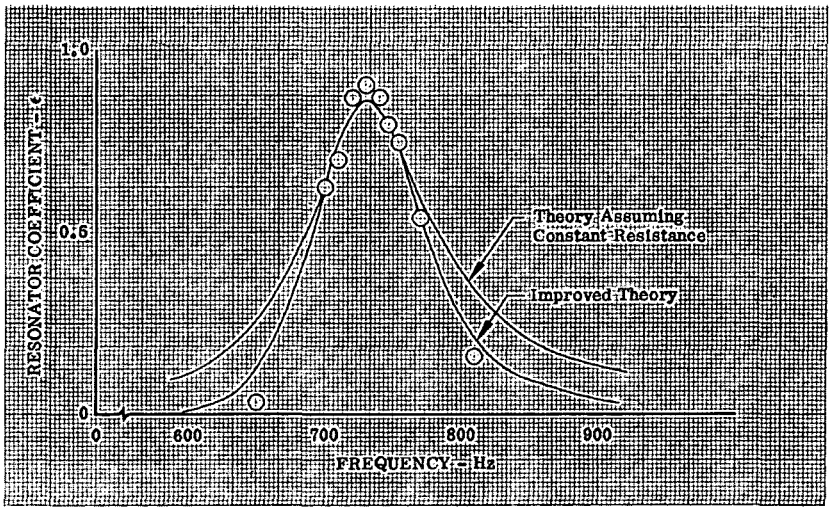

Figure 8. Comparison of Experimental Data from Single Resonator With Nonarray Design Theories — DF 90638

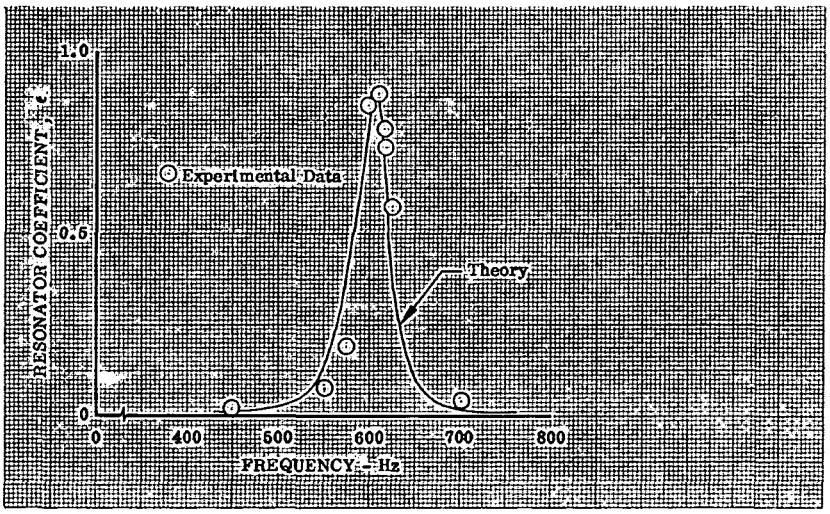

Figure 9. Comparison of Experimental Data from Quarter-Wave Tube With Design Theory — DF 90639

It was concluded that if the resistance coefficient and the effective length correction factor can be specified for a given device, the nonarray theory can be used to accurately predict the resonator coefficient at resonance. Futhermore, the off-resonance coefficients can be predicted with sufficient accuracy for design purposes by either assuming constant resistance or employing an iterative solution to the impedance equation.

C. LIMITATION EXPERIMENTS

The limitation experiments were conducted to investigate the dimensional limitation of acoustic absorbing devices. Included was an investigation of the transition from Helmholtz resonator to quarter-wave tube, acoustic cavity experiments, aperture diameter and length experiments and resonator interaction experiments.

1. Resonator to Quarter-Wave Tube Transition Experiments

A series of cold flow tests was conducted to study the transition between single resonators and quarter-wave tubes. The reverberation chamber was used as a sound source and the pressure-phase impedance technique was used to obtain data. Test sections consisted of two different resonators with adjustable backing depths; one resonator had a cavity diameter of 1.38 in. and the other 2.90 in. Data were taken at seven different frequencies and at resonance; at each frequency, pressure-phase data were recorded at sound pressure levels of 150, 157, and 165 db.

An analysis was conducted of the impedance data obtained from each element to determine the limits for application of the design theory as the aperture of a single resonator is progressively enlarged until it becomes a quarter-wave tube, and to confirm the results obtained from the quarter-wave tube used in the previous series of experiments.

It was found that there is essentially no transition between the single resonator and the $\lambda/4$ tube; as shown in figure 10 the resistance coefficient averaged 0.37 even when the ratio of aperture-to-cavity diameter approaches 90%. Apparently only a small discontinuity in the aperture of a quarter-wave tube is all that is necessary to cause jet formation during both parts of the cycle.

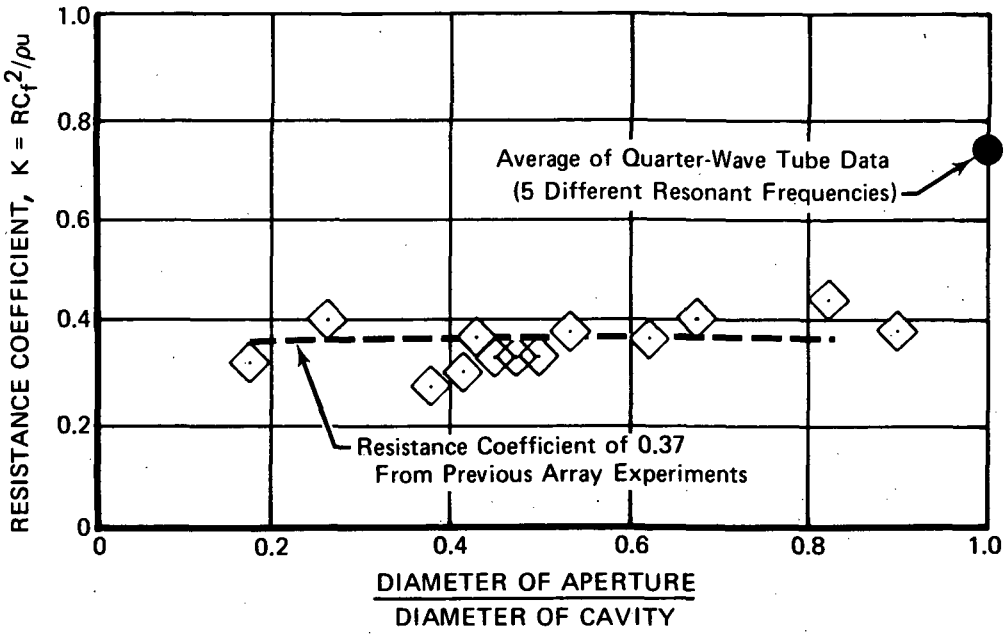

Figure 10. Comparison of Resistance Data from Single Resonators and Quarter-Wave Tubes With Results from Previous Array Experiments DF 61303

The effective length correction factor data were found to be in agreement with theory. In figure 11 the data are shown with a line representing the theory, equation (14); it is worthy of note that the quarter-wave tube correction factors can be predicted with satisfactory accuracy.

2. Acoustic Cavity Experiments

Acoustic cavities are herein defined as those devices that do not cause the incident sound wave to pass through aperture(s) or other restrictions, e.g., porous facings or screens, before entering the cavity. The type of acoustic cavity used for instability suppression has a cavity depth that is near the quarter-wave length of the incident wave.

To study the energy absorbing capabilities of acoustic cavities, cold flow tests of three quarter-wave tubes and three quarter-wave slots were conducted using the high frequency impedance apparatus (Reference 2). The quarter-wave tubes had internal diameters of 0.243 in., 0.305 in., and 0.430 in. and a depth of 1.0 in., which corresponds to the quarter-wave length for a frequency of 3390 Hz. The quarter-wave slots (figure 12) each had the same cross-sectional areas as the quarter-wave tubes, and also had a cavity depth of 1.0 in. The tests were conducted with each cavity by taking pressure-phase data at sound

levels from 140 to 160 db at resonance and also taking data over a range of frequencies from 1800 to 4000 Hz at a constant sound level of 150 db.

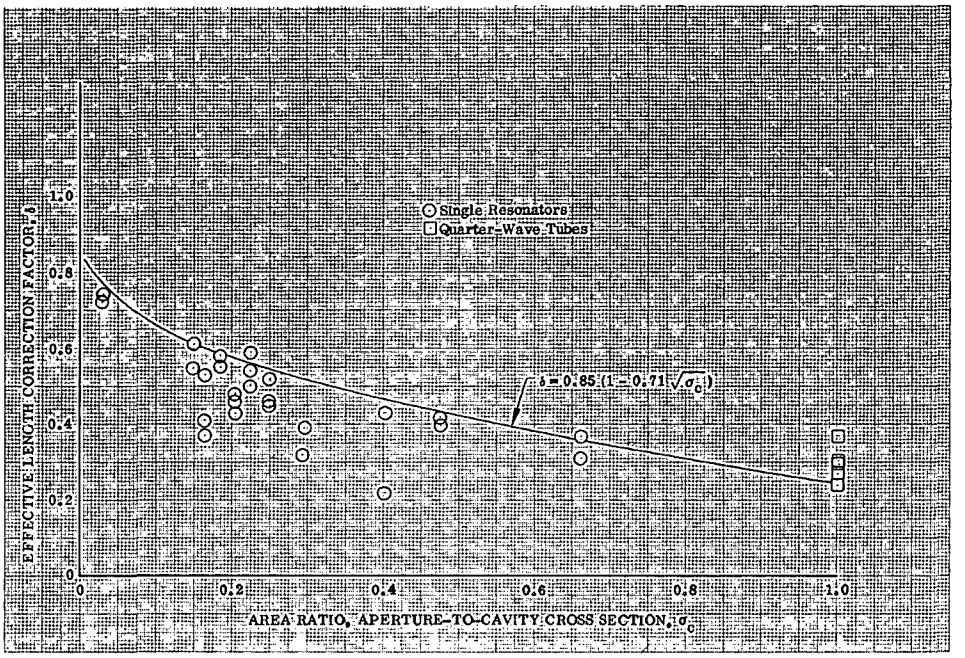

Figure 11. Comparison of Effective Length Correction Factor Data With Theory

DF 90640

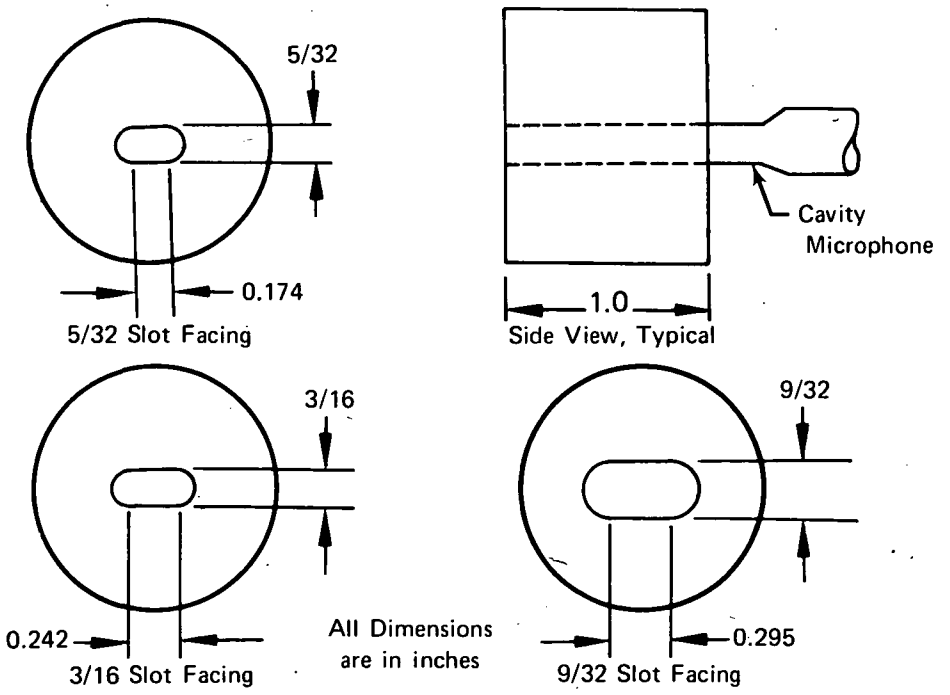

Figure 12. Quarter-Wave Slots Used in Acoustic Cavity Experiments

FD 61304

All of the acoustic cavities were found to have fundamental frequencies lower than that corresponding to their quarter wave lengths. The ratio of the measured fundamental frequency to theoretical was approximately 0.92 for the slots, and slightly lower for the tubes ($\approx$0.9). Quarter-wave cavities have frequencies of resonance that are somewhat lower than theory because the air column in the device oscillates and thus has an overall or effective length that is slightly longer than the cavity depth. For the cavities used in these experiments, the effective length could be approximately determined by

$$L_e = 1.1L$$

where

L = the actual cavity depth

However, as shown previously, the effective length correction factor can be predicted using theory; therefore, a more accurate method of predicting the fundamental frequency of acoustic cavities would be to use equation (14) to compute δ (for acoustic cavities, t = 0). Then use

$$L_e = L + \delta d \tag{57}$$

and

$$f_o = \frac{c}{4L_e} \tag{58}$$

to compute the frequency of resonance. If the device is not circular, an alternative form of equation (57) is

$$L_e = L + 0.96\sqrt{A}\ (1 - 0.71\sqrt{\sigma_c}). \tag{59}$$

Comparisons of the acoustic power absorbed by the slots and tubes showed that at resonance the energy absorbed by slots was greater than that absorbed by tubes even though each had identical open areas and backing depths. (See figure 13.) In addition, it was found that the slots had a lower resistance coefficient (average value of K was 0.53) than tubes for a given sound level, and the slots had average particle velocities approximately twice those of tubes.

From further analysis it was concluded that the difference in peak power absorption between tubes and slots is caused by differences in the local particle

velocities at the edges of the two devices. Because the tube aperture is symmetrical, it has local particle velocities that are uniform around the perimeter. In the slot the smaller dimension controls the local acoustic flow through the aperture, and because this dimension is always less than the tube diameter causes the acoustic flow to be more constricted than in the tube resulting in higher local particle velocities around the slot periphery for a particular incident sound pressure level. Energy absorption is a strong function of the local velocities, hence, the net result of the constriction is to cause the slot to have higher peak absorption.

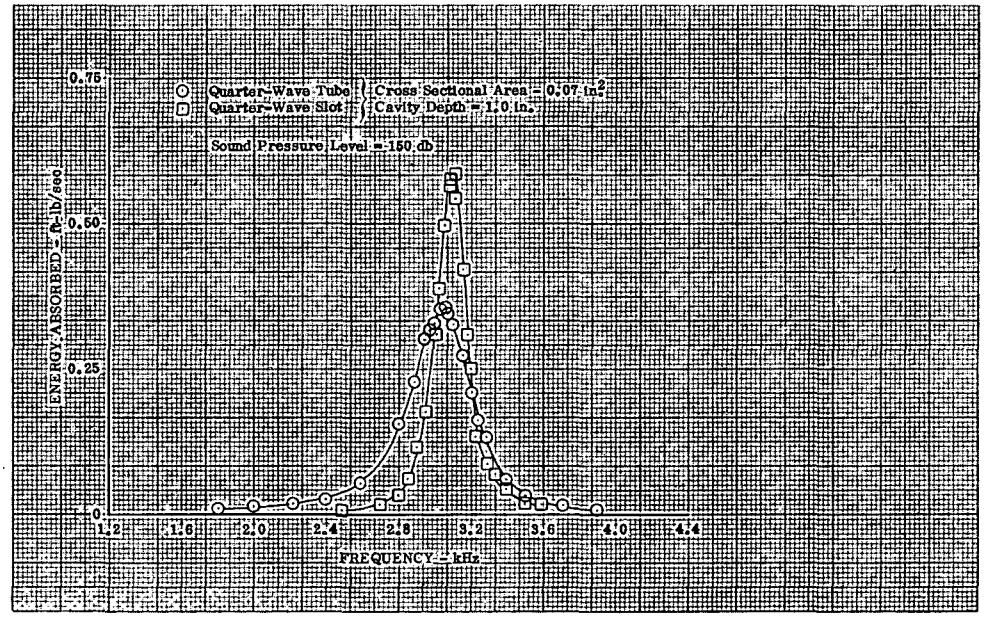

Figure 13. Comparison of the Power Absorbed by a Quarter-Wave Tube and a Quarter-Wave Slot DF 90641

The bandwidth or off-resonance absorbing characteristics of the two devices were also different; as shown in figure 13, absorption with the slot changed with frequency more rapidly than with the tube indicating that the Q value for the slot was higher. These results are to be expected since the Q values of most acoustic devices are inversely proportional to resistance.

The analysis of data from the acoustic cavity experiments was concluded by comparing the acoustic power absorbed by the three sets of quarter-wave tubes and slots with the theoretical absorption of single resonators having the same aperture areas and cavity volumes; results for one set are shown in

figure 14. In every case it was found that for the same sound level and frequency of resonance the equivalent single Helmholtz-type resonator will absorb more acoustic power than either a slot or a tube. This is because, as explained previously, the resonator dissipates energy in the two jets that form during each cycle; but with quarter-wave devices a jet can form only during that part of the cycle when there is flow out of the cavity, therefore less energy can be dissipated.

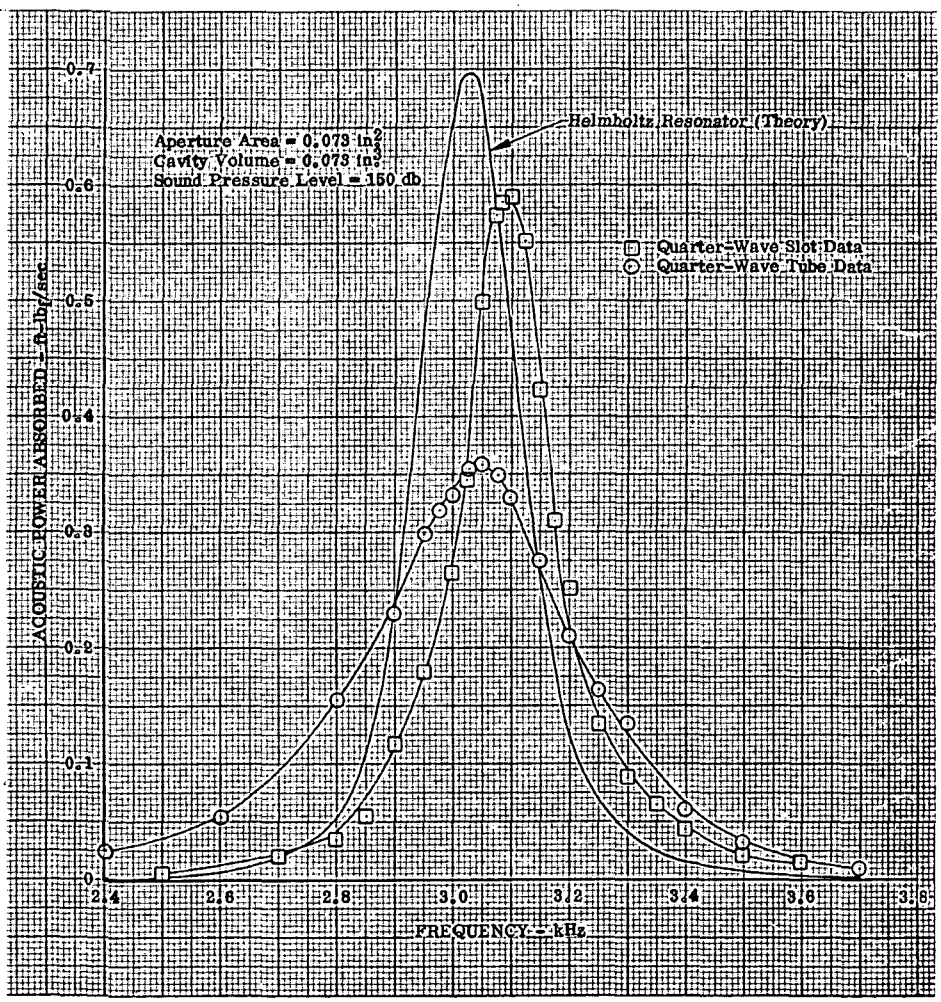

Figure 14. Comparison of Acoustic Absorption Data from a Quarter-Wave Tube and a Quarter-Wave Slot With the Theoretical Absorption of a Single Resonator DF 90642

From the results of this analysis, it is concluded that acoustic cavities are less desirable than resonators for use as rocket combustion stabilizing devices because: (1) for the same cavity volume and aperture area more energy

can be dissipated by a resonator; (2) the inherent narrow band absorbing characteristics and the difficulty in predicting the fundamental frequency make the tuning of acoustic cavities much more critical than that required for resonators. Even if a cavity is precisely tuned for the instability in a given motor and purged with gas of known properties to provide constant sonic velocity, little or no absorption will be obtained if the instability occurs at a slightly different frequency (which often happens).

3. Aperture Diameter Experiments

The objective of this experiment was to determine the diameter limitation of a resonator aperture. A series of pressure-phase experiments was conducted using the reverberation chamber as a sound source. A single resonator with an aperture diameter of 1.25 in. and an adjustable cavity depth of 2.9 in. diameter was used. The cavity depth was decreased in 0.2 in. increments starting at 1.2 in.; data were recorded at the corresponding frequencies of resonance. As the backing depth was decreased the resonance frequency increased causing the wavelength to approach the aperture diameter.

The acoustic data were first analyzed using the ratio of the aperture diameter to wavelength. The resistance coefficient was calculated from equation (55) and the effective length coefficient from equation (56); results are shown in figure 15. The resistance coefficient was constant until the aperture ratio exceeded 0.3, then increased rapidly while the reactance, as represented by the effective length coefficient, increased slightly.

It is known from previous work, Reference 2, that for operation in the nonlinear regime the particle velocity must be greater than 60 ft/sec. Examination of the diameter limitation data revealed that the majority of the orifice velocity values were less than 60 ft/sec; thus a second series of diameter limitation experiments was conducted to obtain data at higher particle velocities. The tests were made with facing samples of 0.375 and 0.182 in. diameter and backing cavity depths varying from 0.90 to 0.05 in. The data were again recorded at the resonance frequency of each configuration as the backing depth was decreased. The results are shown in figure 16; the data from the earlier experiment with orifice particle velocities greater than 60 ft/sec are also included. An increase in resistance coefficient was again noted for the values of $4\ d/\lambda$ greater than 0.3; however, the results also indicated that the resistance coefficients for the 0.182-in. diameter experiments began to increase at

4 d/λ = 0.15. A correlation was then made (figure 17), between the resistance coefficient and the backing cavity depth to aperture diameter ratio. The resistance coefficient was found to be constant until the ratio of backing depth to aperture diameter decreased below 0.8. A second correlation was made to combine the effect of aperture diameter, wavelength, and cavity depth on the resistance coefficient. The results are presented in figure 18, where the resistance coefficient as a function of 4 d/λ L is shown. The data indicate that for values of 4 d/λ L in excess of 1.0 the resistance coefficient deviates significantly from the value used in the design theory (0.37).

A third series of experiments was conducted using the high frequency impedance tube to verify the aperture diameter limitation. The test was conducted using a single aperture having a 0.213 in. diameter and a thickness of 0.125 in. The diameter was chosen so that wall interaction with the source side of the impedance tube would not affect the results. In addition, to prevent the high-frequency fundamental modes of the cavity from introducing error, the tests were conducted without a cavity. The results are shown in figure 19; results of the previous experiments are also included. Data for 4 d/λ in excess of 0.4 could not be obtained because of frequency and sound pressure limitations of the impedance tube.

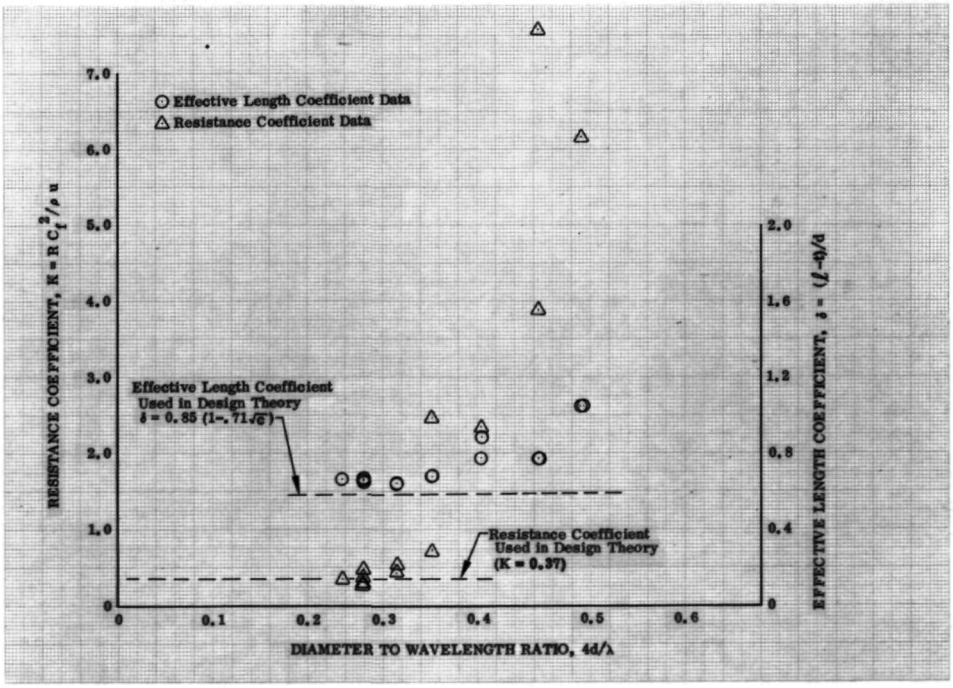

Figure 15. Comparison of the Resistance and Effective Length Coefficients for the First Series of Aperture Diameter Limitation Tests DF 90643

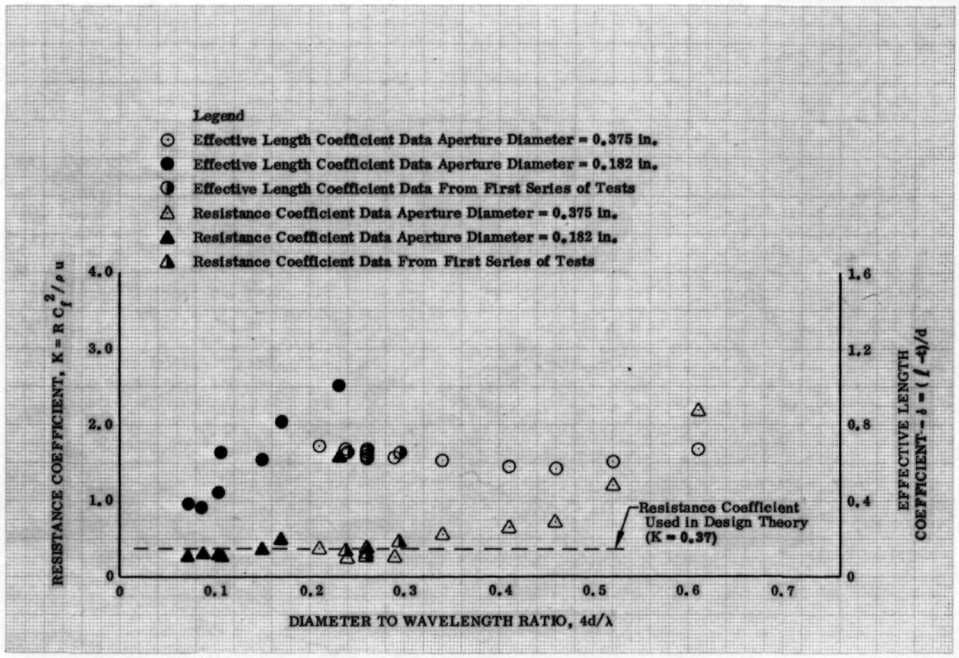

Figure 16. Comparison of the Resistance and Effective Length Coefficient as a Function of Diameter to Wavelength Ratio DF 90644

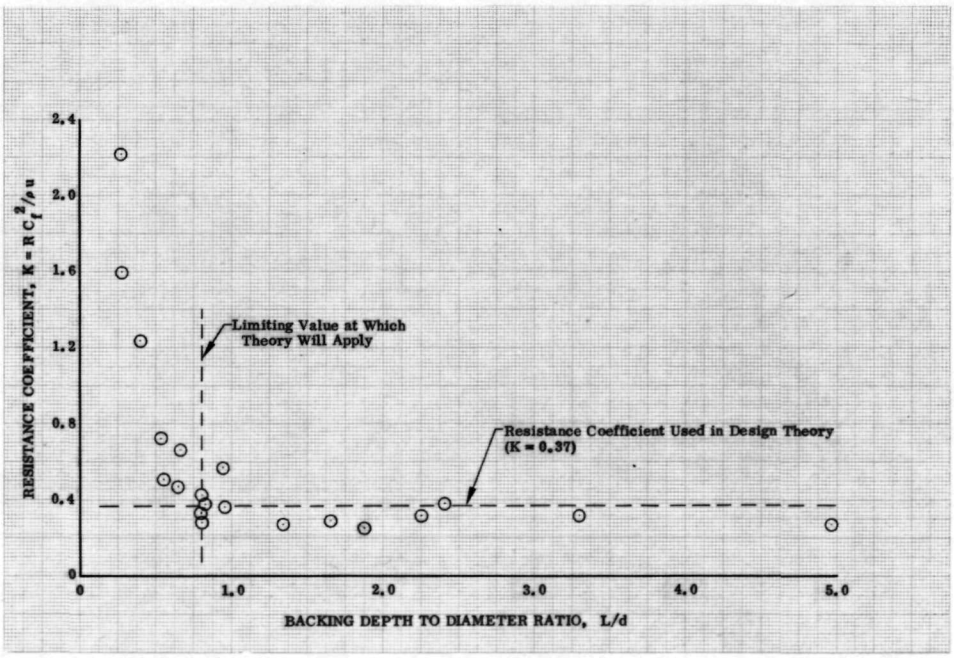

Figure 17. Correlation of Resistance Coefficient Data With Backing Depth to Aperture Diameter Ratio DF 90645

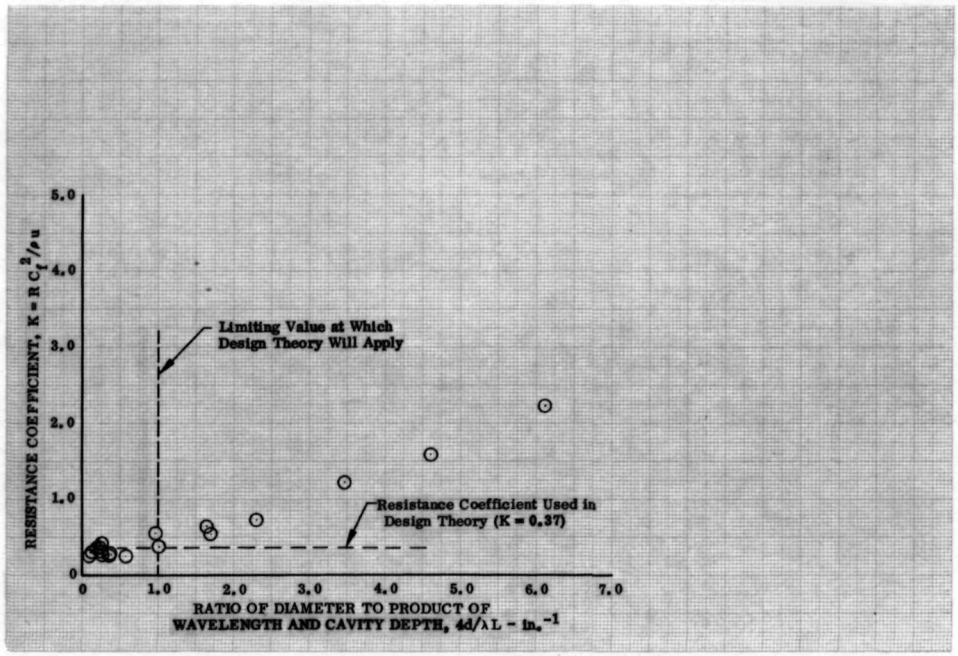

Figure 18. Correlation of Resistance Coefficient Data With Diameter, Wavelength, and Cavity Depth

DF 90646

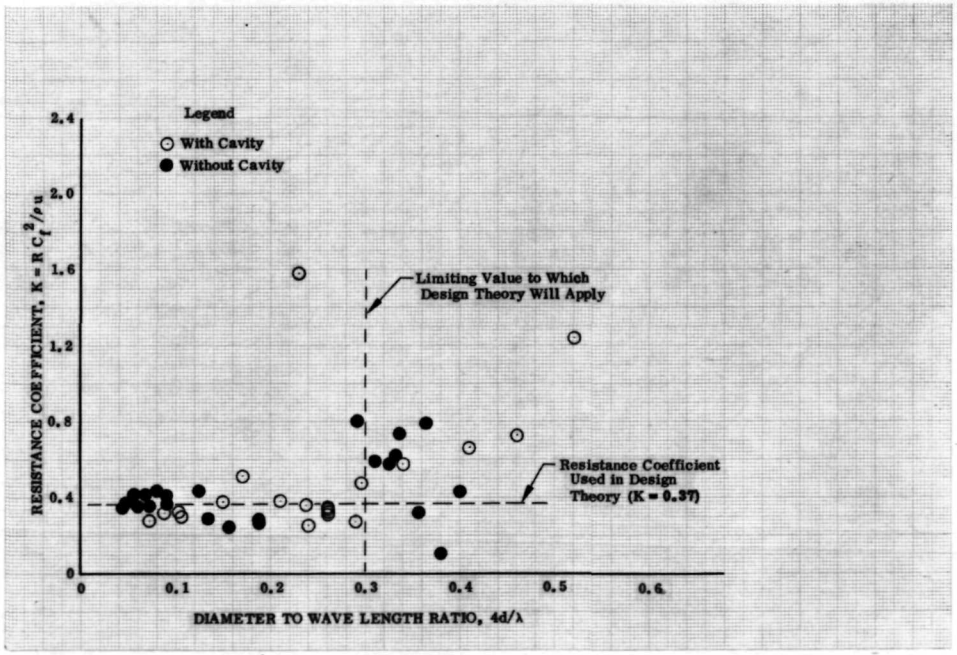

Figure 19. Comparison of Resistance Coefficient Data for Apertures With and Without Cavity as a Function of the Diameter Wavelength Data

DF 90647

The results indicated considerable resistance coefficient scatter was present for values of the diameter to wavelength ratio in excess of 0.3 for the experiment without a cavity; however, the average value of the coefficient between 4 d/λ = 0.3 and 0.4 was 0.55, which is consistent with data from the earlier experiments.

From the results of the limitation experiments it is recommended that apertures of single resonators be designed so that the ratio of aperture diameter to the product of backing depth and quarter-wave length is less than 1.0 at resonance (all dimensions in inches).

4. Aperture Length Experiments

The objective of the experiments was to determine the length limitations of resonator apertures. The high frequency impedance tube was used as a sound source and both the standing wave and the pressure-phase impedance techniques was used to obtain data. Two series of experiments were conducted: (1) data were obtained at resonance for a configuration with apertures shorter than or equal to the quarter-wavelength, and (2) data were obtained with an aperture longer than quarter wavelength.

a. Apertures Shorter Than or Equal to the Quarter-Wavelength

An analysis was conducted of the impedance data obtained to determine the limits for application of the design theory as the aperture length was increased. It was found that the resistance coefficient did not change significantly from the predicted value of 0.37 as the thickness was increased from 0.5 to 3.35 in. (See figure 20.) However, the frequency of resonance predicted by

$$f_o = \frac{c}{2\pi}\sqrt{\frac{\sigma_c}{L\ell}} \tag{60}$$

was found to be increasingly in error as the aperture length was increased.

The error should be expected since equation (60) is obtained from the reactance equation at resonance

$$X = \rho\,\omega\ell - \sigma_c \frac{\rho c^2}{\omega L} = 0 \tag{61}$$

that was simplified from

$$X = \rho c\,\tan\left(\frac{\omega\ell}{c}\right) - \rho c\,\sigma_c \cot\left(\frac{\omega L}{c}\right) \tag{62}$$

by the restriction that $\omega L/c$ and $\omega \ell/c$ be small, so that $\cot \omega L/c = c/\omega L$ and $\tan \omega \ell/c = \omega \ell/c$. As shown in figure 21 this assumption and thus the simplified equation is accurate for values of $\omega \ell/c$ less than 0.4; however, for larger values, which is the case for the longer aperture configurations tested, the error becomes significant.

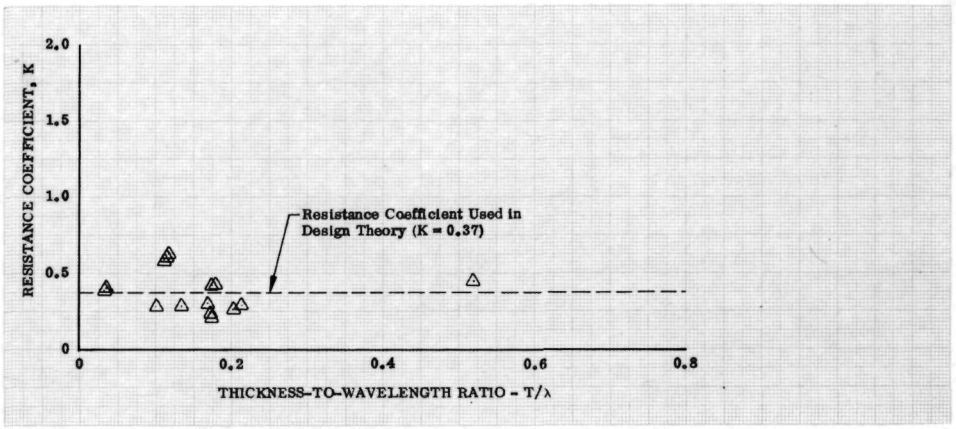

Figure 20. Effect of Thickness on the Resistance Coefficient DF 90648

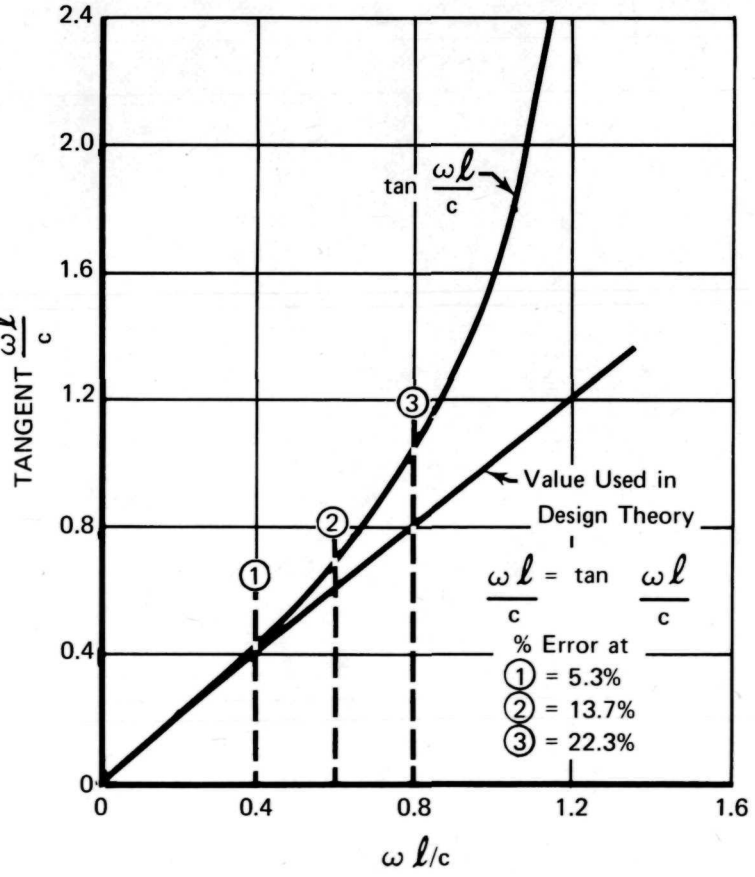

Figure 21. Comparison of Design Theory Assumption for Small Values of $\omega \ell/c$ With Tangent $\omega \ell/c$ FD 61305

A comparison of the resonance frequency from the impedance data and the calculated data using both equation (61) and (62) are shown in table III.

Table III. Results at Resonance for Apertures Smaller Than or Equal to Quarter-Wavelength

Aperture Length, in.	Resonance Frequency Impedance Data, Hz	Resonance Frequency, Equation 61, Hz	Resonance Frequency, Equation 62, Hz
0.5	911	957	915
1.5	923	1009	936
2.0	909	1088	891
2.5	912	1232	909
3.0	910	1590	913
3.15	913	1740	910
3.35	710	1062	733
3.35	704	1012	716

It was concluded from the analysis that the design theory of Section II can be used with reasonable accuracy for values of $\omega\ell/c$ and $\omega L/c$ less than or equal to 0.4, for other values equation (62) should be used in the calculation of the frequency of resonance and the acoustic reactance.

b. Aperture Longer Than a Quarter-Wave Length

An analysis was conducted of the impedance data to determine the effects of apertures longer than a quarter-wave length on absorbing characteristics. The data were obtained for a resonator having a 3.25 in. long aperture with a backing cavity depth of 0.262 in., and an aperture diameter of 0.18 in. The data were obtained at frequencies from 400 to 6000 Hz. Since the values of $\omega L/c$ and $\omega\ell/c$ were at times greater than 0.4 for the frequency range of interest, equation (62) was used to calculate the absorption characteristics of the resonator, i.e., solve for the resonant frequency, f_o, by letting X = 0 and use the equation to compute the reactance at other frequencies. As expected, it was found that in addition to the predicted fundamental mode resonance also occurred at several higher frequencies. The resistance coefficient was found to be approximately 0.37 for the fundamental and for all harmonics. Figures 22, 23, and 24 show comparisons of the experimental data with the theory for reactance, absorption coefficient, and power absorbed, each as a function of frequency.

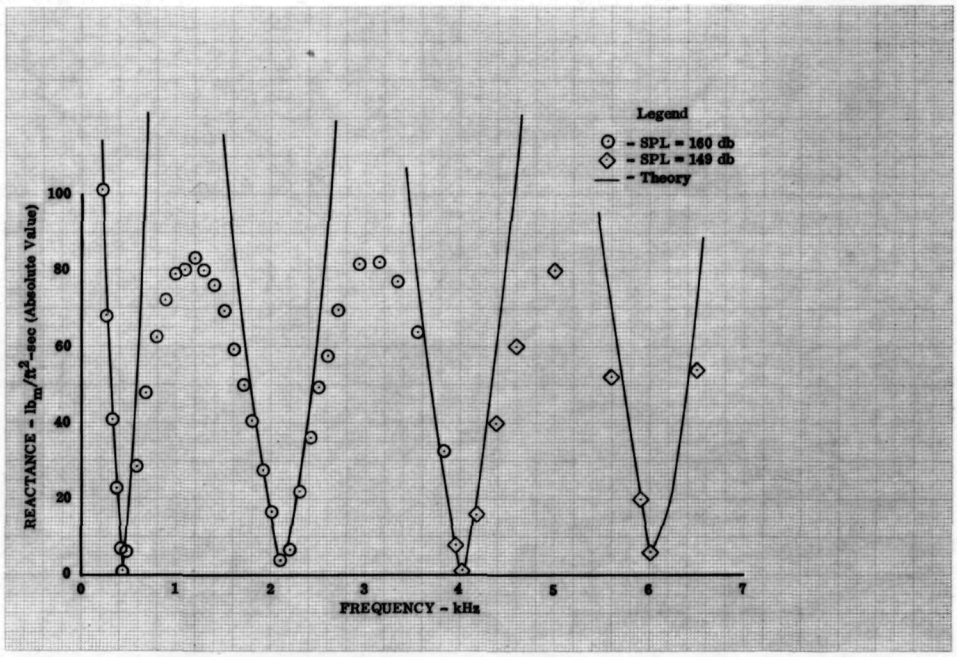

Figure 22. Comparison of Theoretical and Experimental Reactance for the Fundamental Mode and Harmonics of a Single Resonator DF 90649

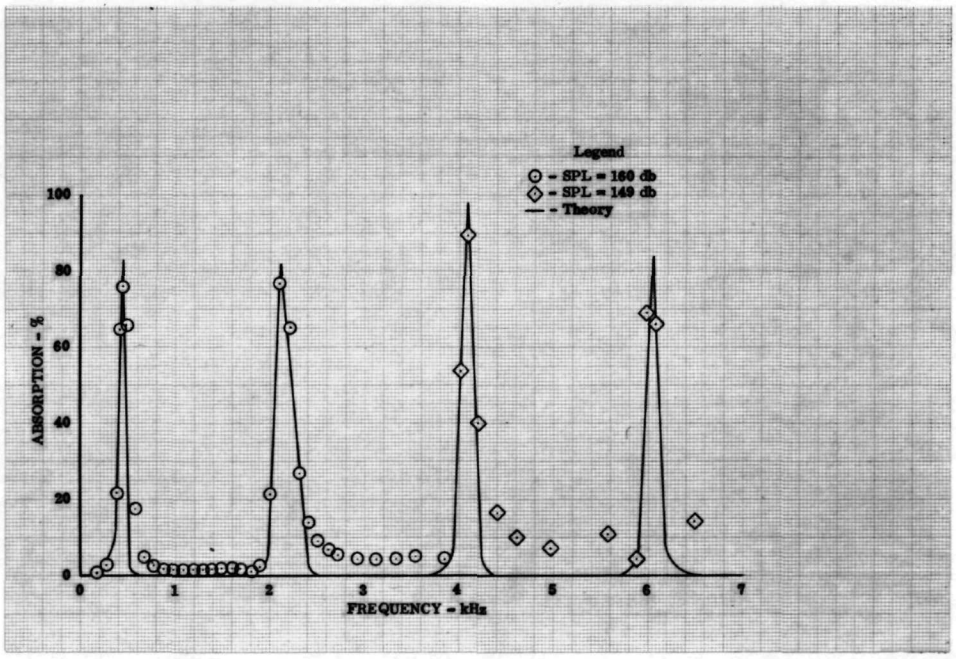

Figure 23. Comparison of Theoretical and Experimental Absorption Coefficients for the Fundamental Mode and the Harmonics of a Single Resonator DF 90650

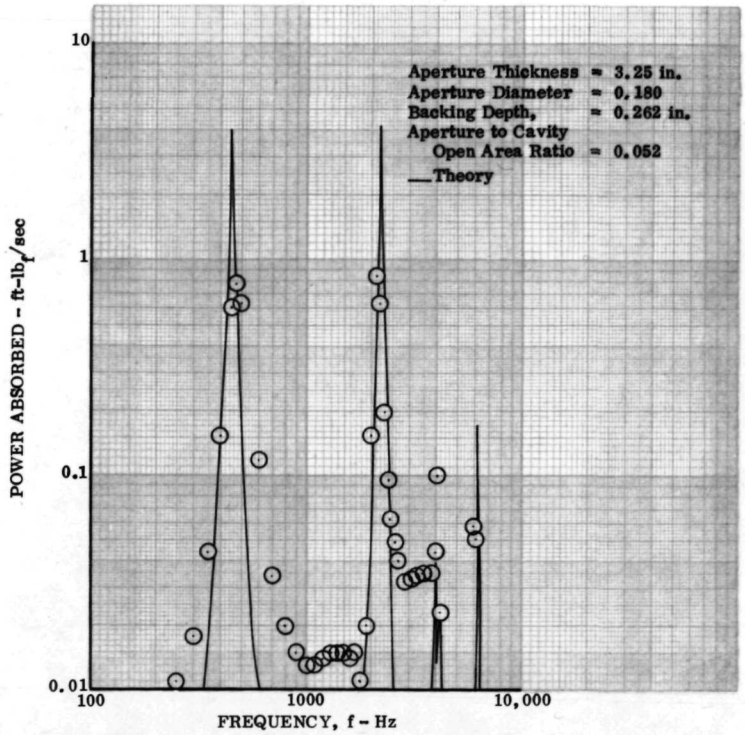

Figure 24. Comparison of Theoretical and Experimental Power Absorbed for the Fundamental Mode and the Harmonics of a Single Resonator DF 90651

It was concluded that apertures longer than a quarter-wave length could be used in the design of acoustic resonators only if equation (62) is used to calculate the acoustic characteristics of the device. This procedure was followed in the formulation of the design computer program of Appendix C. The program will predict both fundamental and harmonic absorbing characteristics if any occur within the specified range of frequencies.

5. Resonator Interaction Experiments

Designers of acoustical absorbers may, for a given aperture area, use a single aperture or two (or more) smaller apertures. Equations (14) and (45), show in theory, that if smaller apertures are used the effective length will also be smaller, resulting in a higher frequency of resonance; thus, to maintain the same frequency of resonance the cavity volume must be increased.

A series of experiments was conducted to investigate the effect of aperture interaction on resonance using a given total aperture area and various numbers of apertures all connected to a central, unpartitioned cavity. The high frequency impedance apparatus was used to perform the experiments; both pressure-phase

and standing wave data were obtained. Five resonator facings having 1, 2, 4, 6, and 25 apertures were used. Each facing had a total open area of 0.026 $in.^2$, a cavity volume of 0.028 $in.^3$, and facing thickness of 0.1 in. The single aperture was tested first; the absorption was measured at resonance. The absorption of the remaining four resonators was then measured at two frequencies, one corresponding to the resonant frequency of the single resonator and at the resonant frequency of the particular resonator. Results are listed in table IV.

Table IV. Results From Single and Multiple Aperture Experiments

Number of Apertures	Resonance Frequency, Hz	Acoustic Power Absorbed, ft-lbf/sec	
		at Resonance	at 1580 Hz
1	1580	0.52	0.52
2	1620	0.52	0.52
4	1780	0.52	0.52
6	1810	0.52	0.50
25	1940	0.52	0.42

It was found that within the limits of experimental error, all the resonators except the 25 aperture facing had the same absorption at resonance, and as the number of apertures was increased, the frequency of resonance increased. Thus, as theory predicts, to maintain resonance at the original frequency, i.e., 1580 Hz, the cavity volume would have to be increased. These results show that if the resonator is not cavity volume limited, the number of apertures used to produce a given open area is immaterial. However, if the resonator is volume limited, highest absorption for a given cavity volume will be obtained with the fewest number of apertures.

The 25 aperture facing had significantly lower abosrption at 1580 Hz than any other facing because of the usual decrease in absorption that occurs at frequencies far from resonance, and because of the small diameter of the apertures (0.037 in.). It is believed that as the aperture diameter is decreased below approximately 0.050 in. the boundary layer begins to fill a significant percentage of the open area. The average oscillatory velocity in the boundary layer is lower than the main stream particle velocity, thus less energy dissipation takes place and a decrease in the bandwidth characteristics occurs. For this reason, perhaps 0.050 in., is a realistic lower limit for aperture diameter.

Experiments were next conducted to determine how a single resonator is affected when a second identical but completely separate resonator is brought into the near vicinity. Each resonator had a single aperture with a diameter of

0.125 in., a cavity diameter of 0.305 in., and a backing depth of 0.875 in. The experiments were conducted using the high-frequency impedance apparatus; data were obtained from standing wave and phase measurements, i.e., the resonant frequency was determined by varying the driver input frequency until a phase angle of 90 deg was obtained between the cavity and facing microphones. Standing wave data were then taken at resonance over a range of sound levels from 145 to 170 db.

It was found, as shown in table V, that introduction of the second element had essentially no effect on the frequency of resonance.

Table V. Results of Interaction Experiments

Sound Pressure at Facing, db	Frequency of Resonance, Hz	
	One Resonator	Two Resonators
144.6	1941	1940
149.8	1944	1944
154.9	1954	1954
159.4	1961	1961
164.9	1974	1977
169.8	--	2009

The theory predicts that because neither the cavity open area ratio nor the aperture diameter were changed in the experiment, the frequency of resonance should have remained constant. The slight change in f_o with sound pressure, while certainly within the accuracy demonstrated by the correlation of figure 11, is not predictable by theory. For this reason it is suggested that nonarray absorbers, like liner arrays, be designed for good off-resonant absorption characteristics.

Comparison of other data from the experiment showed excellent agreement. The power absorbed data are shown in figure 25 and the particle velocity data are shown in figure 26.

The final series of interaction experiments was conducted to determine if placing the aperture of an absorbing device in a corner, e.g., in a rocket chamber at the intersection of the chamber wall and the injector face, would affect its acoustical characteristics. Two resonators having four apertures of the same diameter and length connected to a common, unpartitioned cavity were fabricated for testing in the high-frequency impedance tube. The first, the control resonator, had the apertures arranged so that each was as far removed from

the sidewall of the tube and from the other apertures as possible; the apertures of the second were located as close to the sidewalls as possible (figure 27). Each resonator was tested over a range of frequencies from 1550 to 1900 Hz at a sound level of 160 db.

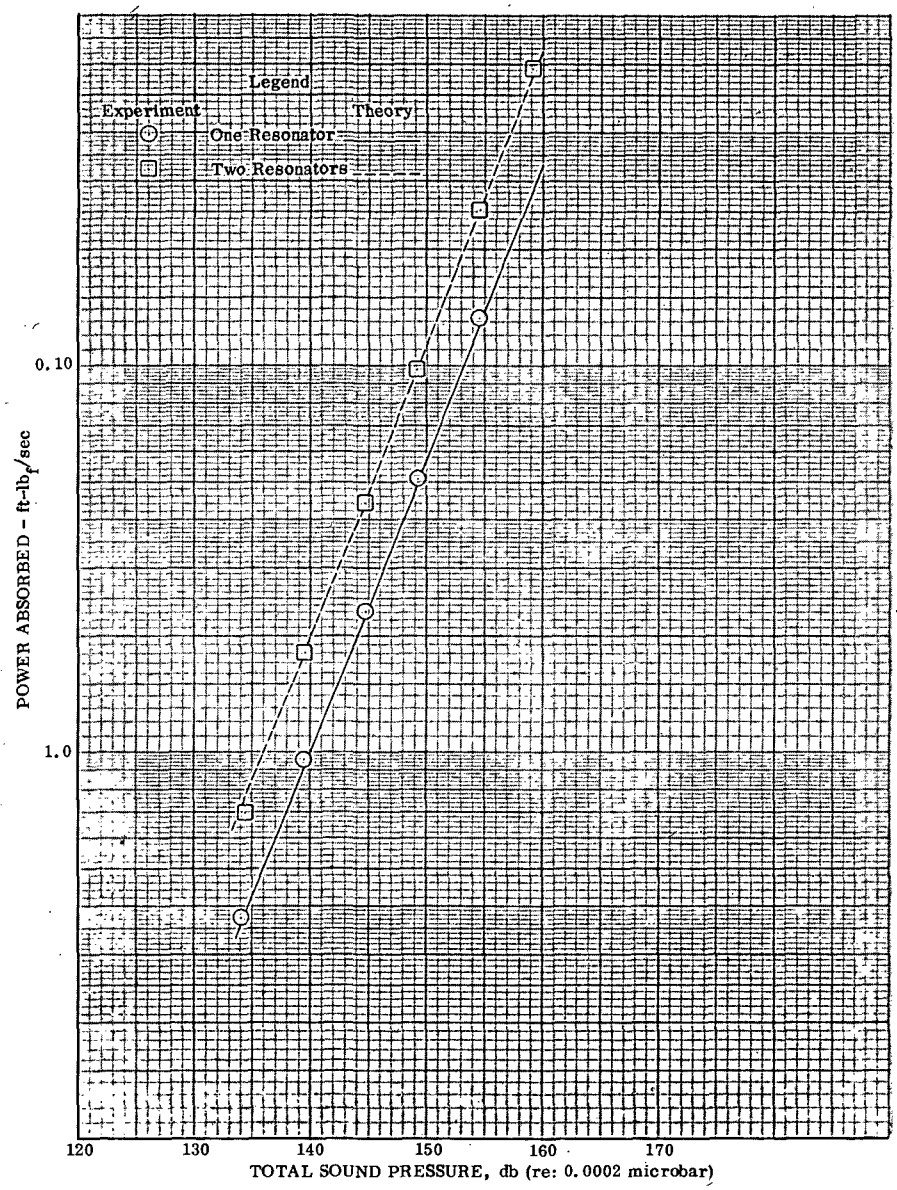

Figure 25. Results of Interaction Experiments With Identical Resonators DF 90652

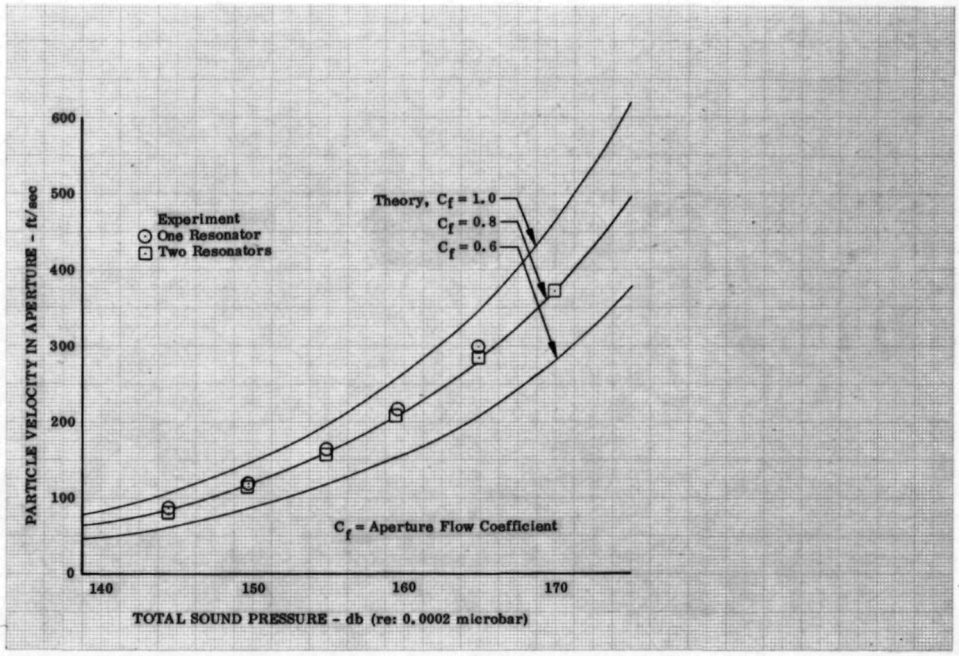

Figure 26. Comparison of Aperture Particle Velocity from Interaction Experiments With Theory DF 90653

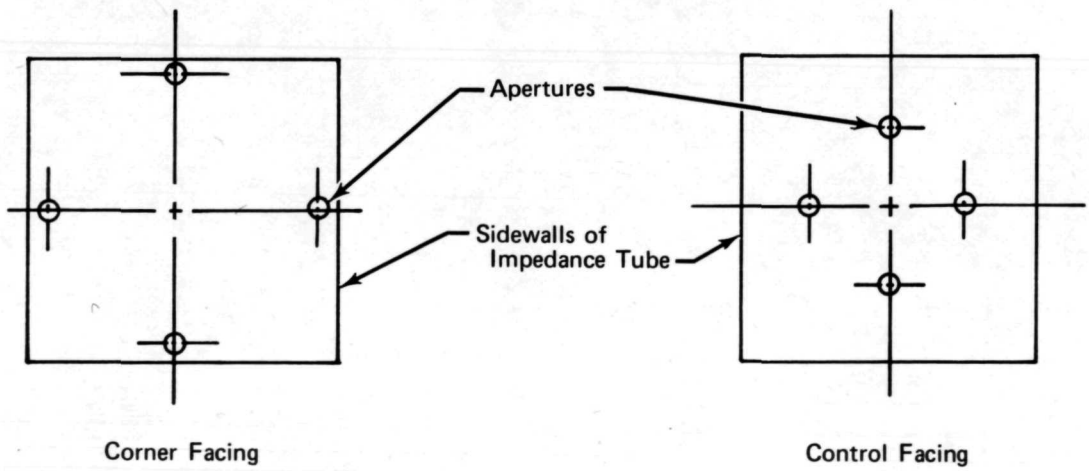

Figure 27. Types of Facings Used in Corner Interaction Experiment FD 62348

Two effects of placing the apertures in the corners were noted: (1) a 2.5% increase in resonance from 1785 to 1830 Hz, and (2) more significantly, an increase in the power absorbed (figure 28). The small change in resonance is believed to be within the limits of experimental accuracy, and therefore, cannot be attributed to the presence of the corner walls, but, the increase in absorption can. Analysis of the absorption data revealed that the increase was produced primarily by a slight increase in particle velocity. Apparently, the corner walls produced a funneling effect, which resulted in slightly higher acoustic velocities during both halves of the acoustic cycle.

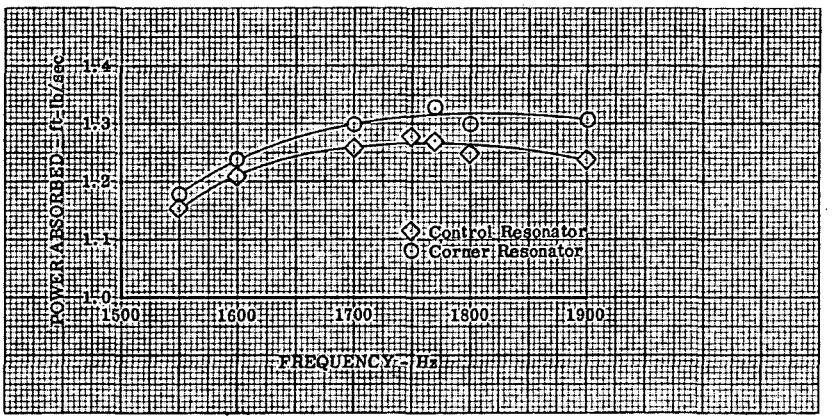

Figure 28. Absorption Data from Corner Interaction Experiment DF 90654

For the design analysis of resonators that are to be placed within one diameter of a wall or other structure, e.g., injector face baffle, it is suggested that a value of 0.34 be used for the resistance coefficient, which will cause the predicted absorption and particle velocity to be increased by the corresponding amount observed in the above experiments.

SECTION IV
APPLICATION OF THEORY-SAMPLE CALCULATIONS

The following calculations illustrate a method for determining the optimum physical dimensions of a nonarray absorbing device using the theory of Section II and the cold flow experimental results of Section III. The device will be single resonator; as shown in Section III, these devices are more desirable than any other type of nonarray absorber because of their inherently greater energy dissipation and broad-band absorbing characteristics. It is assumed that the resonator will be located in the wall of a rocket chamber so that the aperture is near the injector faceplane, the most effective location for such a device, and that the combustor will be operating at the following conditions:

Chamber Pressure, $P = 60$ psia
Combustion Gas Temperature, $T_c = 6000°R$
Frequency of Oscillations to be Damped, $f_o = 6000$ Hz
Gas Constant of Combustion Products, $\Upsilon = 45.7$ ft lb_f/lb_m °R
Ratio Specific Heats, $\gamma = 1.2$

Past experience (Reference 5) has shown that the aperture gas temperatures are significantly lower than the combustion gas temperature even if no liner cooling or purge flows are used. Although it is extremely difficult to predict the aperture gas temperatures in an untested motor, a reasonable assumption based on past experience is that the aperture gas temperature is one-half the combustion gas temperature, i.e.,

$$T_a = \frac{1}{2} T_c = 3000°R$$

Using perfect gas relations the density and sonic velocity in the aperture are

$$\rho = \frac{P}{\Upsilon T_a} = \frac{(60)(144)}{(45.7)(3000)} = 0.063 \text{ lb}_m/\text{ft}^3$$

$$c = \sqrt{\gamma g \Upsilon T_a} = \sqrt{1.2(32.2)(45.7)(3000)} = 2300 \text{ ft/sec}$$

A. RESONANCE CALCULATIONS

The fundamental frequency of the resonator will be the same as the frequency of the oscillations to be damped. At that frequency the wavelength is

$$\lambda_o = c/f_o = 2300/6000 = 0.383 \text{ ft},$$

the wave number is

$$k = 2\pi f_o/c = \frac{2\pi}{\lambda_o} = 16.41 \text{ ft}^{-1}$$

and the critical spacing is

$$b = 0.4\lambda_o = 1.84 \text{ in.}$$

For maximum effectiveness, as many resonators as possible should be installed in the chamber; the above spacing is the minimum distance between the centers of adjacent apertures with separate resonator volumes. If for any reason the spacing must be closer than the minimum, the array theory (Reference 2) must be used for the design.

1. Aperture Area

For the zero flow case, i.e., negligible net velocity past and/or through the aperture, the optimum aperture area is found using equation (33).

$$A_{opt} = \frac{\lambda_o^2}{2\pi}\sqrt{\frac{B}{\gamma}\left(\frac{p_i}{P}\right)}$$

By definition $B = KC_f^{-2}$ where K is the resistance coefficient (0.37 for circular apertures*) and C_f is the aperture discharge coefficient. For this case it is assumed that the aperture will have slightly rounded edges so that $C_f = 1$; then

$$B = 0.37(1)^{-2} = 0.37.$$

As suggested in Reference 5, the resonator is designed for the maximum pressure amplitude allowed for combustion to be considered stable, usually 5% of the static pressure. Using 5% for this example we have $p_i/P = 0.05$ and the optimum area is

$$A_{opt} = \frac{\lambda_o^2}{2\pi}\sqrt{\frac{B}{\gamma}\left(\frac{p_i}{P}\right)}$$

$$= \frac{(0.383)^2}{2\pi}\sqrt{\frac{0.37}{1.2}\ (0.05)} = 0.0029 \text{ ft}^2$$

For a single circular aperture

$$d_{opt} = \sqrt{\frac{4A_{opt}}{\pi}} = \sqrt{\frac{4(0.0029)(144)}{\pi}} = 0.73 \text{ in.}$$

*For other values of K see page 2.

If the optimum diameter is too large for the particular application it is possible to use two or more smaller apertures with a common cavity to obtain the required open area because, as shown in Section III, the number of apertures used to produce a resonator of given total open area with a common unpartioned cavity is immaterial unless the device is cavity volume-limited. If cavity volume is limited, highest absorption will be obtained with the fewest number of apertures. If multiple apertures are used it is recommended that all be contained within a surface area no larger than $\lambda_o/2\pi$.

The above restraints will cause, in some cases, applications in which it will not be possible to have aperture areas as large as required for optimum absorption. Then, a smaller area should be used and the resonator coefficient evaluated using the following procedure. For this example assume that a single aperture of diameter 0.5 in. can be installed. The aperture area is

$$A = \pi d^2/4 = \frac{\pi(0.5)^2}{4(144)} = 0.00136 \text{ ft}^2$$

and the dimensionless radiation resistance, computed using equation (30), is

$$\theta_r = k^2 A/2\pi = \frac{(16.41)^2(0.00136)}{2\pi} = 0.0583$$

Compute the dimensionless particle velocity, which for zero flow is also the dimensionless dissipation resistance, using equation (29)

$$m_o = -\frac{\theta_r}{2} + \sqrt{\left(\frac{\theta_r}{2}\right)^2 + \frac{2B}{\gamma}\left(\frac{p_i}{P}\right)}$$

$$= -\left(\frac{0.0583}{2}\right) + \sqrt{\left(\frac{0.0583}{2}\right)^2 + \frac{2(0.37)(0.05)}{1.2}}$$

$$= 0.1492$$

The ratio of the two resistances, β_o is

$$\beta_o = R/R_r = m_o/\theta_r = 0.149/0.0576 = 2.56$$

and the resonator coefficient is computed using equation (11), which for resonance (X = 0) becomes

$$\epsilon_o = 4\beta_o/(\beta_o + 1)^2$$

$$= \frac{4(2.56)}{(3.56)^2} = 0.808$$

If the optimum aperture area had been used in the above calculations, $\beta_o = 1$ and $\epsilon_o = 1$ would have resulted. Note that a 53% reduction in the aperture area decreased the resonator coefficient by only 19%. For the remainder of the computations necessary to design the resonator the optimum aperture area will be used, i.e., d = 0.73 in.

2. Cavity Backing Depth

The cavity backing depth is determined using the results of the Section III Limitation Experiments. From those experiments it was found that

$$\frac{4d}{\lambda_o L} \leq 1 \text{ in.}^{-1}$$

is a limiting condition, which as in this case, if the diameter and wavelength are known, can be used to determine the minimum backing depth, L_{min}; e.g., rearranging the above equation produces

$$\frac{4d(1 \text{ in.})}{\lambda_o} \leq L$$

hence,

$$L_{min} = \frac{4d(1 \text{ in.})}{\lambda_o}$$

Substituting the known values (d and λ_o) gives

$$L_{min} = \frac{4(0.73)}{(0.383)(12)} = 0.635 \text{ in.}$$

3. Aperture Length and Cavity Open Area Ratio

The last two physical dimensions of the resonator may be obtained by first assuming a value for the aperture effective length, ℓ, and then using the reactance equation (62) at resonance to determine the cavity open area ratio, σ_c. The aperture length, t, can then be computed from the effective length equation that applies for the particular device being designed.

At resonance, equation (62) can be written as

$$\sigma_c = \tan\left(\frac{2\pi f_o \ell}{c}\right) \tan\left(\frac{2\pi f_o L}{c}\right)$$

Assuming a value of 0.35 in. for ℓ and using $L = L_{min} = 0.635$ produces

$$\sigma_c = \tan\left[\frac{2\pi(6000)(0.35)}{(2300)(12)}\right]\tan\left[\frac{2\pi(6000)(0.635)}{2300(12)}\right]$$

$$= \tan(0.478)\tan(0.87)$$

$$= (0.518)(1.188) = 0.613$$

It must be remembered that σ_c is the area ratio between the aperture cross section and that of the cavity, not between the aperture and the chamber surface area. If the cavity has a circular cross section the diameter will be

$$d_c = d_a/\sqrt{\sigma_c}$$

$$= 0.73/\sqrt{0.616}$$

$$= 0.93 \text{ in.}$$

For this case (a resonator with zero flow) the applicable effective length equation is $\ell = t + \delta d$ where δ is computed from equation (14)

$$\delta = 0.85(1 - 0.71\sqrt{\sigma_c})$$

$$= 0.85(1 - 0.71\sqrt{0.616}) = 0.377$$

Then, by rearranging the effective length equation, $\ell = t + \delta d$, to obtain

$$t = \ell - \delta d$$

$$= 0.35 - 0.377(0.73) = 0.075 \text{ in.}$$

The effective length equations for use with flow or for quarter-wave cavities are found on pages 9 and 28, respectively.

B. OFF-RESONANCE CALCULATIONS

The absorbing characteristics of the resonator must now be determined by computing the resonator coefficient at frequencies other than resonance.

The quality factor is first computed using equation (40)

$$Q = \frac{\lambda_o \ell}{A(\beta_o + 1)}$$

$$= \frac{0.383(0.35)}{0.0029(2)(12)}$$

$$= 1.926$$

Assuming the resistance constant, the resonator coefficient can then be calculated using equation (42)

$$\epsilon = \frac{4\beta_o}{(\beta_o + 1)^2} \quad \frac{1}{1 + Q^2(\zeta - 1/\zeta)^2}$$

where ζ is the frequency ratio f/f_o.

In table VI are the resonator coefficients calculated using this equation for frequencies from 5000 to 7000 Hz and in figure 29 is a comparison of the calculated resonator coefficients with those computed for the example case using the computer program of Appendix C. The only difference between the two sets of calculations is the computer program does not use the constant resistance assumption to compute the off-resonance absorbing characteristics. (See page 11.)

Table VI. Calculated Values of Resonator Coefficient Based on Constant Resistance Assumption

Frequency, Hz	Frequency Ratio, f/f_o	Resonator Coefficient
5000	0.833	0.67
5200	0.867	0.77
5400	0.90	0.86
5600	0.933	0.93
5800	0.967	0.98
6000	1.00	1.00
6200	1.03	0.98
6400	1.07	0.94
6600	1.10	0.88
6800	1.13	0.81
7000	1.167	0.74

C. FLOW EFFECTS

A flow of gas past or through the apertures can, if the Mach number is high enough, cause an increase in the dissipation resistance and a change in the resonator coefficient.

1. Past-Flow Resonance Calculations

The following calculations show a method of evaluating the flow effects assuming a net flow past the aperture with a Mach number, (M_p) of 0.15.

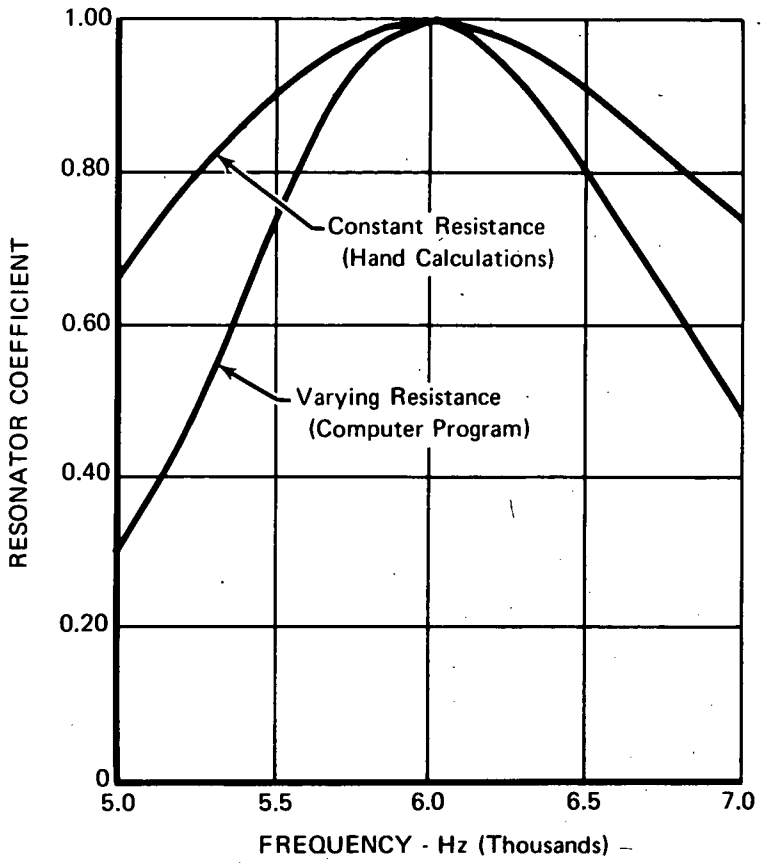

Figure 29. Comparison of Computed Resonator Coefficients for Example Case FD 62364

The Mach number of the oscillatory flow in the aperture at resonance is found using the definitions

$$m_o = B\frac{u_o}{c}$$

where m_o is computed using equation (29). Again using the optimized aperture area in equation (30)

$$\theta_r = k^2 A_{opt}/2\pi$$
$$= (16.4)^2\,(0.0029)/2\pi)$$
$$= 0.124$$

which when substituted in equation (29) gives

$$m_o = -\frac{\theta_r}{2} + \sqrt{\left(\frac{\theta_r}{2}\right)^2 + \frac{2B}{\gamma}\left(\frac{p_i}{P}\right)}$$

$$= -\frac{0.124}{2} + \sqrt{\left(\frac{0.124}{2}\right)^2 + \frac{2(0.37)(0.05)}{1.2}}$$

$$= 0.124$$

and an aperture Mach number of

$$\frac{u_o}{c} = \frac{m_o}{B} = \frac{0.124}{0.37} = 0.335$$

To determine if the past-flow can be ignored the left side of inequality (45) is evaluated:

$$\frac{M_p}{u_o/c}\left(\frac{T_c}{T_a}\right)^2 = \frac{0.15}{0.335}\left(\frac{6000}{3000}\right)^2 = 1.8$$

Because, as explained in Section II, the resulting value is greater than 1.5, the effects of flow cannot be ignored. The dimensionless dissipation resistance with flow is computed using equation (46).

$$\frac{R_p}{\rho c} = \frac{BM_p}{3}\left(\frac{T_c}{T_a}\right)^2 + \frac{B}{2}\left(\frac{u_o}{c}\right)$$

$$= \frac{0.37(0.15)}{3}\left(\frac{6000}{3000}\right)^2 + \frac{0.37}{2}(0.335)$$

$$= 0.136$$

The value of β_p is

$$\beta_p = \frac{R_p}{R_r} = \frac{(R_p/\rho c)}{\theta_r} = \frac{0.136}{0.124} = 1.1$$

which gives a resonator coefficient of

$$\epsilon_p = \frac{4\beta_p}{(\beta_p + 1)^2} = \frac{4(1.1)}{(2.1)^2} = 0.997$$

Thus, in this case, the flow has almost no effect on the resonator coefficient. If the coefficient had been reduced below approximately 0.5 a new optimum aperture area should be found using equation (48) and the design procedure of subsection A repeated.

Because a different effective length equation is used with past-flow the aperture length must be recomputed. The effective length with past-flow, equation (44), can be written as $\ell_p = t + 0.375\ \delta d$ where all variables, except t, are the same as the zero flow case; therefore,

$$t = \ell_p - 0.375\ \delta d$$

$$= 0.35 - 0.375(0.377)\ (0.73)$$

$$= 0.245 \text{ in.}$$

Hence, the most significant effect of the past-flow is the increase in aperture thickness (from 0.075 to 0.245 in.) required to cause resonance to occur at the same frequency.

2. Through-Flow, Resonance Calculations

If there is a net flow of Mach number M_T through the aperture such that $M_T < u_o/2c$, the effect on absorbing characteristics can be ignored. If not, a procedure similar to that necessary with past-flow is followed except that equations (50) and (51) are used to compute the resistance and optimum area, respectively, and the effective length equation for zero flow, equation (14), is used.

3. Off-Resonance Calculations

The off-resonance absorbing characteristics with either type of flow are identical to those of the zero-flow case with one exception: with past-flow the quality factor, equation (40), is computed using the effective length from equation (44).

APPENDIX A
REVERBERATION TEST TECHNIQUES

A reverberation room is a highly sound-reflective room in which special care has been taken to make the sound field as diffuse as possible. Reverberation tests are used to measure the absorption characteristics of acoustical materials. As the samples are relatively large and the sound is incident at random angles, the measurement of absorption is made, in many cases, under conditions closer to those of an actual installation than those in tests for impedance and absorption of acoustical materials by the impedance tube method.

The sound that persists and decays in an enclosed space after the sound source has stopped is called reverberation. The rate of decay, D, in decibels per second is given by (Reference 4)

$$D = \frac{1.087\ a\ c}{V_c} \tag{A-1}$$

where a is defined as the total absorptive power of the room of volume V_c expressed as

$$a = \sum_i \alpha_i S_i \tag{A-2}$$

with α_i as the respective absorption coefficient representing the fraction of randomly incident energy absorbed by different surfaces of area, S_i, forming the interior walls of the reverberation chamber.

In accordance with the original proposal of Sabine (Reference 9), who defined the reverberation time, T_{60}, as the time required for the level of the sound in the room to decay to 60 db, then

$$T_{60} = \frac{60}{D} = \frac{55.2\ V_c}{a\ c} \tag{A-3}$$

In acoustical engineering it is customary to express V_c in cubic ft, and a in Sabines, where the Sabine is an absorption unit representing a surface capable of absorbing sound at the same rate as does 1 ft^2 of perfectly absorbing surface. Introducing for air, c - 1125 ft/sec, equation (A-3) becomes the Sabine reverberation equation

$$T_{60} = \frac{0.049\ V_c}{a} \tag{A-4}$$

According to ASTM Standards (Reference 10), the Sabine equation is based on certain assumptions that must be fulfilled if measurements are to have meaning. These assumptions are: the sound field is diffuse before and during decay; the decay in decibels is essentially linear; and the measured decay rate is independent of the position of microphone or test sample.

If an acoustical material having an absorptive surface, S, is suspended inside the reverberation chamber, a new reverberation time T'_{60} will equal (Reference 4)

$$T'_{60} = \frac{0.049\ V_c}{a + S\alpha_e} \tag{A-5}$$

where α_e is the effective absorption coefficient of the material being investigated. If equations (A-4) and (A-5) are combined to eliminate a, then

$$\alpha_e = \frac{0.049\ V_c}{S}\left(\frac{1}{T'_{60}} - \frac{1}{T_{60}}\right) \tag{A-6}$$

In recent years (Reference 11), there has been a tendency to standardize the quantity measured in reverberation chambers as the decay rate of sound pressure level in decibels per second rather than the reverberation time. Under such circumstances, it is advantageous to use equation (A-3) to eliminate T_{60} and T'_{60} from equation (A-6) and, thereby, obtain

$$\alpha_e = \frac{0.00081\ V_c}{S}(D' - D) \tag{A-7}$$

where D' is the measured decay rate when the material being investigated is present in the reverberation chamber, and D is that measured when it is absent.

For some acoustical elements, e.g., quarter-wave tubes, slots, and non-array resonators, the surface area can only be arbitrarily defined, hence, a measure of total absorption is more meaningful. The total absorption, W, of the element can be obtained from reverberation data using the equations

$$W = 0.049\ V_c\left(\frac{1}{T'_{60}} - \frac{1}{T_{60}}\right) \tag{A-8}$$

and

$$W = 0.00081\ V_c\,(D' - D) \tag{A-9}$$

The principal limitations of the reverberation room method are found at low frequencies (below 250 Hz), where the rooms are too small, and at frequencies above 4000 Hz, where absorption by the test media itself limits the accuracy. The works of Knudsen (Reference 12) on absorption caused by water vapor in the air pointed out the reason for the short reverberation times at high frequencies. Since water vapor absorption may be different when the empty room reverberation tests are made than they are when absorbing room tests are made, it can be a serious cause of inaccuracy, in addition to errors inherent in measurements of rapid decays. Consequently, steps should be taken to provide a constant humidity for tests made in reverberation chambers. In addition, diffraction or area corrections are important for small porous test samples having high absorption. Parkinson (Reference 13) discussed experimental evidence of the diffraction problem, and, in 1939, Chrisler (Reference 14) gave the basis of empirical area correction used by the National Bureau of Standards.

Comparisons of reverberation and calculated absorption coefficients have been made (Reference 15), in which the calculated values were based on impedance tube data. Close agreement is possible (figure A-1) for absorbers designed so that air can flow only normal to the surface. These absorbers are of the resonant-type, consisting of perforated panels with air space backing and are identical to full-array liners used in rocket chambers. Although excellent agreement exists between the reverberation and impedance tube technique of measuring absorption characteristics, the reverberation method has a definite advantage in that non-array devices of any shape or configuration can easily be tested.

Reverberation chambers, according to ASTM Standards (Reference 10), should be constructed of massive, nonresonant materials. The average absorption coefficient of the chamber walls, determined by empty room measurements, should be less than 0.05 at all frequencies of interest, after allowance has been made for atmospheric absorption. The room must be isolated sufficiently from outside noises and vibrations to keep the ambient noise level 15 db below the lowest level at which measurements are made. A pentagonal chamber configuration is recommended in MIL-STD-810B, Method 515. A chamber of this configuration is best proportioned to produce, as closely as possible, a diffuse sound field, with a sound energy density that is very nearly uniform throughout the enclosure as required for use of Sabine's equation in calculating absorption.

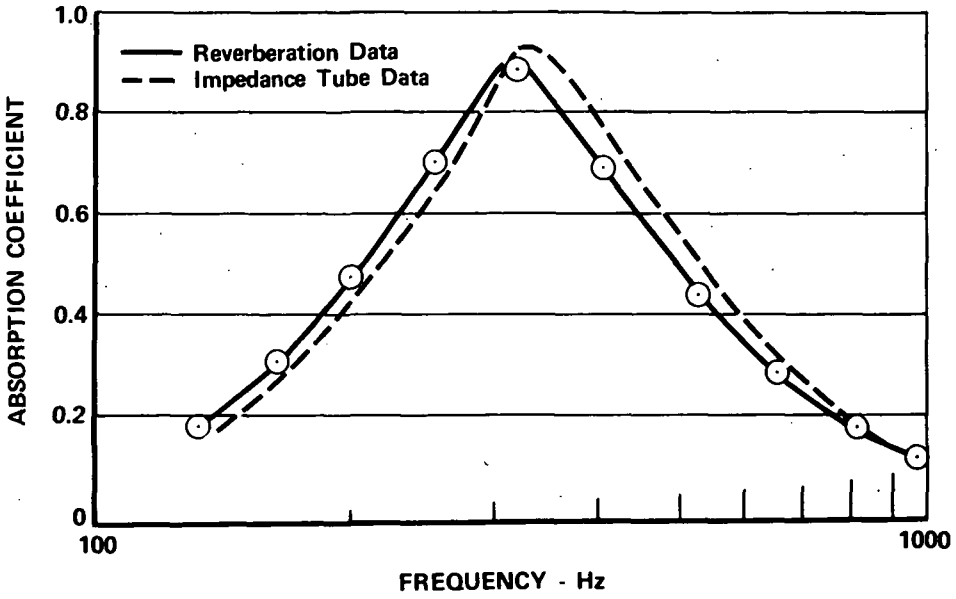

Figure A-1. Comparison of Absorption Coefficients Obtained from Reverberation and Impedance Tube Tests FD 40091

Test specimen size should be limited to a maximum value not to exceed 10% of the chamber volume. Excessively small specimens should also be avoided to minimize the effects of diffraction (References 12, 13, and 14). The test specimen may be placed on the floor for larger chambers (over 8000 ft^3), but for smaller chambers it is necessary to suspend the specimen from the ceiling to ensure that the sound is randomly incident on the surface of the specimen.

The sound source used to drive the chambers should be one or more high intensity speakers mounted preferably in the trihedral corners of rectangular rooms. It may be necessary in oddly shaped and small chambers to mount the speakers outside the chamber and to introduce the test signal through exponential horns mounted through the side walls of the chamber.

Various experimenters (References 16 and 17) have tried to determine the best test signals to use when performing reverberation experiments. Pure tones, frequency modulated warble tones, combinations of pure tones (multitones), bands of pink noise, and pistol-shot noise have all been investigated. Use of a pure tone signal is not recommended because of a number of normal modes of vibration will be excited and, during the decay period, each of these normal modes assumes its own decay rate, resulting in beats that can cause irregular overall decay rates. (See figure A-2.) No general agreement has

been reached as to which signal is best but, based on comments of Schultz (Reference 18), the use of either a warble tone or bands of white noise is suitable for accurate measurements of reverberation time.

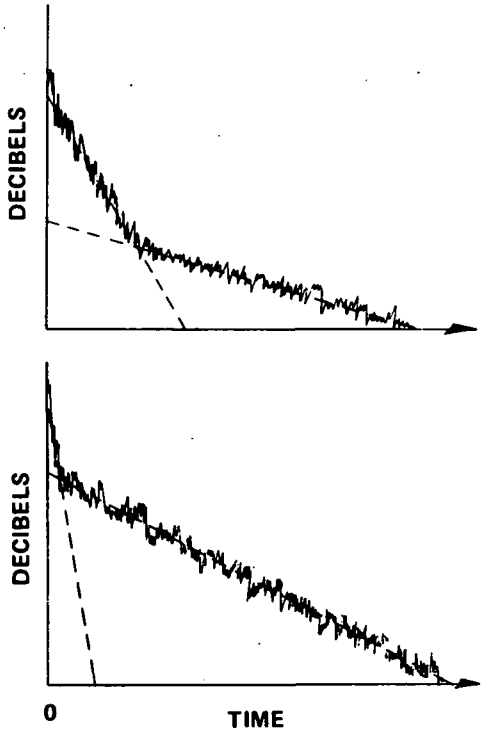

Figure A-2. Decay Curves With Double Slopes Produced by Normal Modes of Vibration With Different Decay Rates FD 40088

Typical electronic equipment used in reverberation measurements is shown in a block diagram of figure A-3. A tracking generator produces a pure tone signal, which is then input into a frequency modulator to produce a warble tone output. The warble tone signal is then amplified and introduced into the reverberation chamber through two high-intensity loudspeakers. Four microphones are located throughout the chamber to determine if the sound field is diffuse and to provide decay rates for various locations in the chamber as recommended by ASTM Standards (Reference 10). The microphone signal is then passed through a narrow band filter center at the same frequency as the pure tone signal. A logarithmic potentiometer is then used to convert the filter microphone signal to a dc output, which is recorded on a graphic recorder in the form of decibels versus time. A high speed oscillograph recorder could be used to give an accurate measurement of a 20-db drop occurring in a matter of tenths of a second. The graphic recorder thus provides a paper-tape record of the decay

of sound in the reverberation room (figure A-4). Repeated measurements of the decay rate under the same conditions should be expected to show some scatter. In making reverberation tests, therefore, it is necessary to make several decay curves for each mean frequency tested and also for each position of the microphone. From the data an average reverberation decay rate is obtained and used in equation (A-7) or equation (A-9) to calculate the absorption characteristics of the test specimen.

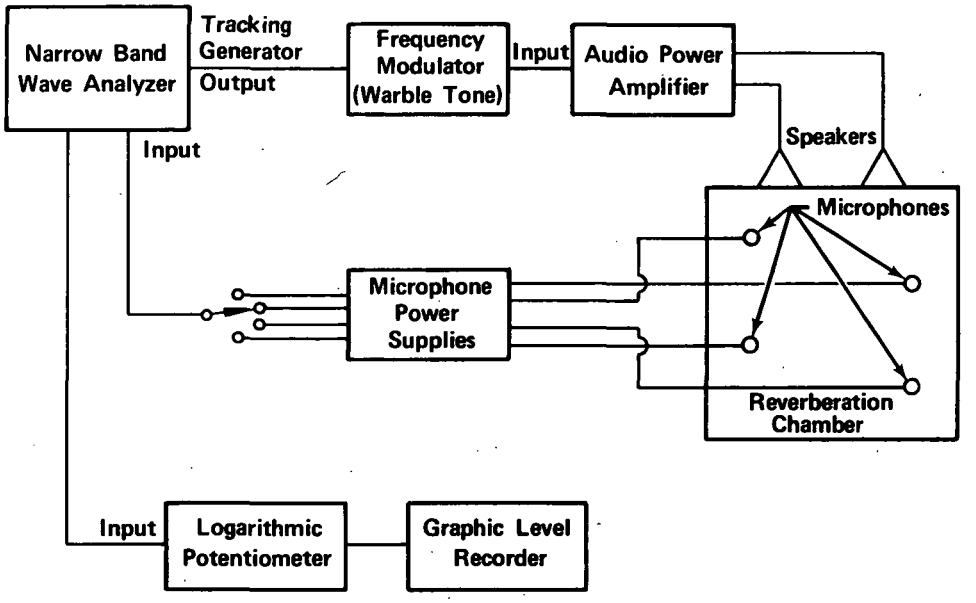

Figure A-3. Schematic of Instrumentation Used for Measurement of Decay Time in a Reverberation Test — FD 40084

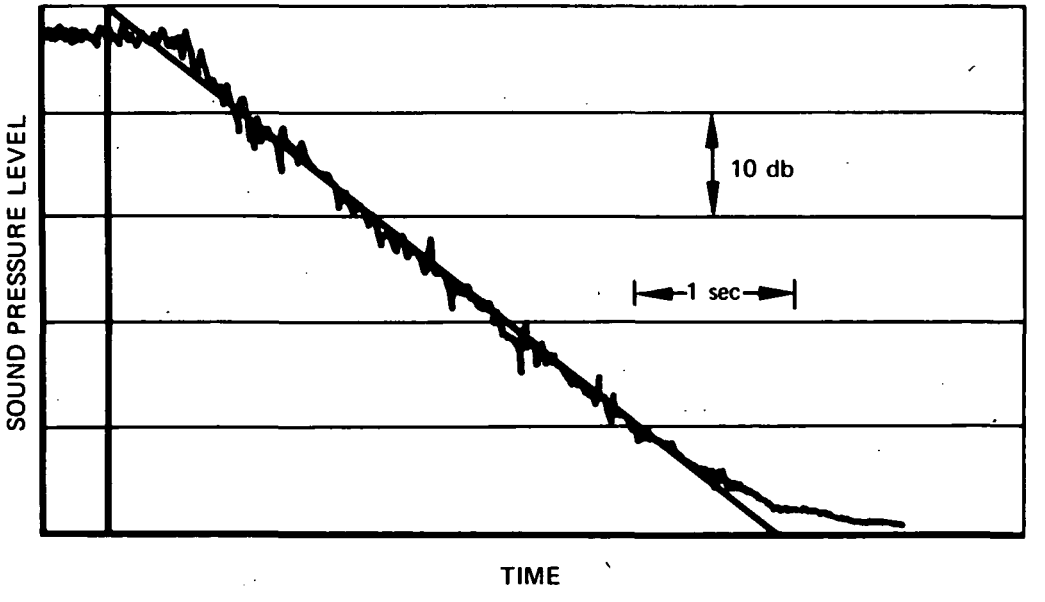

Figure A-4. Typical Graphic Record of the Decay of Sound in a Reverberation Chamber — FD 40090A

APPENDIX B
GENERAL PRESSURE-PHASE DATA REDUCTION EQUATIONS

The following equations were used to determine the impedance of acoustical devices from measurements of the sound pressure directly in front of the aperture, P_1, in the cavity, P_2, and phase difference, ϕ, between P_1 and P_2. The device must consist of a cavity of uniform cross sectional area, A_c, and arbitrary length, L, exposed to an incident sound wave through an aperture of cross sectional area A no larger than that of the cavity.

Impedance

$$Z = \frac{\sigma_c \rho c}{\sin k L} \left(\frac{P_1}{P_2}\right) (\sin\phi + i \cos\phi) \tag{B-1}$$

Resistance (real part of Z)

$$R = \frac{\sigma_c \rho c}{\sin k L} \left(\frac{P_1}{P_2}\right) \sin\phi \tag{B-2}$$

Reactance (imaginary part of Z)

$$X = \frac{-\sigma_c \rho c}{\sin k L} \left(\frac{P_1}{P_2}\right) \cos\phi \tag{B-3}$$

Particle Velocity in Aperture (peak)

$$u = \frac{\sqrt{2}\ g P_2 \sin k L}{\sigma_c \rho c} \tag{B-4}$$

Power Absorbed

$$W = \frac{A_c P_1 P_2 g (\sin k L) \sin\phi}{2 \rho c} \tag{B-5}$$

Resistance coefficient defined by $R = K \rho u C_f^{-2}$

$$K = \frac{\rho}{\sqrt{2}\ g} \left(\frac{\sigma_c\ c\ C_f}{\sin k L}\right)^2 \left(\frac{P_1}{P_2}\right) \frac{\sin\phi}{P_2} \tag{B-6}$$

Effective Aperture Length

$$\ell = \frac{\sigma_c}{k \sin k L} (\cos k L - (P_1/P_2) \cos\phi) \tag{B-7}$$

APPENDIX C
DESIGN COMPUTER PROGRAM

In this Appendix is contained a digital computer program that computes the theoretical acoustic absorbing characteristics of nonarray devices. The program was written in FORTRAN IV for the IBM 1130 computer. The contents appear in the following order:

1. Input Format
2. Output Symbol Nomenclature
3. Sample Input
4. Source Program Listing
5. Output for Sample Cases

The sample input sheet may be used as input for a program test case; results identical to those of the Example Cases should be obtained.

1. Input Format

CARD	COLS	VARIABLE	DESCRIPTION
1	01-05	NCASE	NO. OF COMPLETE SETS OF INPUT
2	01-80	TITLE	ANY TITLE INFORMATION
3	01-10	PRESS	STATIC PRESSURE (PSIA)
	11-20	GASCN	APERTURE GAS CONSTANT (LBF-FT/LBM-R)
	21-30	TEMP	APERTURE GAS TEMPERATURE (RANKINE)
	31-40	TEMPC	COMBUSTION GAS TEMPERATURE (RANKINE)
	41-50	GAMA	RATIO SPECIFIC HEATS, APERTURE GAS
	51-60	CF	APERTURE DISCHARGE COEFFICIENT
	61-70	T	APERTURE LENGTH (INCH)
	NOTE--	FOR QUARTER WAVE TUBE USE INPUT T=0.0	
	71-80	L	BACKING CAVITY DEPTH (INCH)
4	01-10	D	APERTURE DIAMETER (INCH)
	11-20	SIGC	APERTURE-TO-CAVITY OPEN AREA RATIO
	21-30	FMIN	MINIMUM FREQUENCY OF INTEREST (HZ)
	31-40	DELF	FREQUENCY INCREMENT (HZ)
	41-50	FMAX	MAXIMUM FREQUENCY (HZ)
	51-60	SPLN	MIN PRESSURE RATIO, PEAK INCIDENT AMPLITUDE-TO-STATIC
	61-70	DELP	PRESSURE RATIO INCREMENT
	71-80	SPLM	MAX. PRESSURE RATIO
5	01-10	MP	MACH NO. OF FLOW PAST APERTURE
	11-20	MT	MACH NO. OF FLOW THRU APERTURE
	21-30	FO	FREQUENCY OF RESONANCE (HZ)-IF BLANK THE FUNDAMENTAL FREQ OF THE ABSORBER WILL BE COMPUTED.

NOTE--- ALL CARDS (EXCEPT 1) MUST BE INPUT NCASE TIMES ---

2. Output Symbol Nomenclature

VARIABLE	DESCRIPTION
FREQ	FREQUENCY (HZ)
RFREQ	RATIO OF FREQUENCY TO RESONANT FREQ.
RESIS	DISSIPATION RESISTANCE/(DENSITY * SONIC VELOCITY
REACT	REACTANCE /(DENSITY * SONIC VELOCITY)
RADRX	RADIATION RESISTANCE /(DENSITY * SONIC VELOCITY)
UORFX	ORIFICE PARTICLE VELOCITY (FT/SEC)
BETAX	RESISTANCE RATIO, DISSIPATION-TO-RADIATION
RCOEF	RESINATOR COEFFICIENT
POWAB	POWER ABSORBED (FT-LBS/SEC)
CRITA	RATIO, ORIFICE DIAMETER TO QUARTER WAVE-LENGTH AND BACKING CAVITY DEPTH (1./IN.)

PWA 10169 REV. 2-82

FORTRAN CODING FORM

SHEET _____ OF _____

ANALYST _____ ENGINEER _____ EXT _____

JOB NO. _____ COST CONTROL NO. _____

C	NO.	X	FORTRAN STATEMENT	LABEL
	2		EXAMPLE CASE, NO FLOW	
			60. 45.7 3000. 6000. 1.2 1. .075 .636	
			.73 .6131 5000. 100. 7000. .05 1. .05	
			.0 .0 .0	
			EXAMPLE CASE, PAST FLOW	
			60. 45.7 3000. 6000. 1.2 1. .245 .636	
			.73 .6131 5000. 100. 7000. .05 1. .05	
			.15 .0 .0	

4. Source Program Listing

```
      SUBROUTINE SOLVM (FUNCT,YACT,X,TOL,DELA,YCAL)
      DEL=DELA
      KPAS = 1
      I=1
   10 YCAL=FUNCT(X)
      IF(ABS((YCAL-YACT)/YCAL)-TOL)1,1,2
    2 GO TO (3,4) ,KPAS
    3 GO TO (5,6),I
    5 I=2
      YSTOR=YCAL-YACT
      XSTOR=X
      IF (YCAL-YACT) 7,1,8
    7 KFLAG=1
   15 X=X+DEL
      GO TO 10
    8 KFLAG=2
   16 X=X-DEL
      GO TO 10
    6 KPAS=2
      Y=YCAL-YACT
      IF(Y*YSTOR)30,1,11
   11 IF(ABS(YSTOR)-ABS(Y)) 12,1,13
   12 DEL = -DEL
   13 YSTOR = Y
      XSTOR = X
      GO TO (15,16),KFLAG
    4 Y=YCAL-YACT
      IF(Y*YSTOR)17,1,18
   18 YSTOR = Y
      XSTOR=X
      GO TO (19,20),KFLAG
   19 X=X+DEL
      GO TO 10
   20 X=X-DEL
      GO TO 10
   17 DEL=DEL/10.
   30 GO TO (21,22),KFLAG
   21 X=XSTOR+DEL
      GO TO 10
   22 X=XSTOR-DEL
      GO TO 10
    1 CONTINUE
      RETURN
      END
// DUP
*STORE       WS  UA  SOLVM
// JOB T
// FOR
*ONE WORD INTEGERS
      FUNCTION FUNKL(X)
      REAL L
      COMMON L,XLEFF,SIG
      Z=L/12.
      W=XLEFF/12.
      FUNKL=SIG*COS(X*Z)*COS(X*W)/SIN(X*Z)/SIN(X*W)
      RETURN
```

```
      END
// DUP
*STORE       WS  UA  FUNKL
// FOR
*ONE WORD INTEGERS
      FUNCTION FUNKU(X)
      REAL L
      COMMON L,XLEFF,SIG,RRD,XD,PIPP
      FUNKU = X*X*(( X+RRD)**2 + XD**2) / PIPP**2
      RETURN
      END
// DUP
*STORE       WS  UA  FUNKU
// FOR
*IOCS(CARD,1132 PRINTER)
*ONE WORD INTEGERS
**      DECK 13172
      EXTERNAL FUNKL, FUNKU
      REAL L,KP,MP,MT,KO,MO,KL,KOL,KT
      DIMENSION TITLE(20)
      COMMON L,XLEFF,SIG,RADRX,REACT,PIPP
   99 FORMAT (I5)
  100 FORMAT(8E10.0)
      READ(2,99) NCASE
      DO 406 MWH=1,NCASE
      READ(2,101) TITLE
  101 FORMAT(20A4)
      READ(2,100) PRESS,GASCN,TEMP ,TEMPC,GAMA,CF,T,L
      READ(2,100) D,SIG ,FMIN,DELF,FMAX,SPLN,DELP,SPLM
      READ(2,100) MP,MT,FO
      P1=SPLN
      G=32.1725
      PI=3.1416
      PI2=6.2832
      CF2= CF*CF
      XK2=.37
      YACT=1.
      TOL=.001
      DEN=144.0*PRESS/GASCN/TEMP
      SONIC=SQRT(GAMA*GASCN*TEMP*G)
      APARE=PI*(D**2)/4.0
      XLEFF=T+.85*D*(1.-.71*SQRT(SIG))
      IF(FO) 9,8,9
    9 ANGLE=PI2*FO*L/12./SONIC
      XLEFF=SIG*SONIC/PI2/FO*COS(ANGLE)/SIN(ANGLE)*12.
      IF(T) 32,32,53
   32 XK2=2.*XK2
      GO TO 53
    8 IF(MP) 10,11,10
   10 XLEFF=T +.375*(.85*D*(1.-.7*SQRT(SIG)))
   11 IF (T) 5,1,5
    1 FO = SONIC*12./4./(L+XLEFF)
      XK2=2.* XK2
      GO TO 53
    5 FO = SQRT( SIG/L/XLEFF) *12.* SONIC/PI2
      KP=PI2*FO/SONIC
      X=KP
      DELA=X/4.0
```

```
      CALL SOLVM (FUNKL,YACT,X,TOL,DELA,YCAL)
      FO=X*SONIC/PI2
   53 KO= PI2*FO/SONIC
  303 WRITE(3,201) TITLE
  201 FORMAT('1' 1X,20A4,//32X'GAS PROPERTIES'/)
      WRITE(3,202) PRESS,TEMP,GASCN,GAMA,DEN,SONIC
  202 FORMAT(10X'STATIC PRESSURE (PSIA)'F48.3/
     110X'APERTURE GAS TEMP (DEG. R)'F44.1/
     210X'GAS CONSTANT (LBF*FT/LBM/R)'F43.3/
     310X'RATIO OF SPECIFIC HEATS'F47.3/
     410X'GAS DENSITY (LBM/FT**3)'F47.4/
     510X'GAS SONIC VELOCITY(FT/SEC)'F44.1  )
      WRITE(3,203) TEMPC,MP,MT
  203 FORMAT(10X'COMBUSTION GAS TEMP (DEG R)' F43.1 /
     110X'MACH NO OF FLOW PAST APERTURE' F41.3 /
     210X'MACH NO OF FLOW THRU APERTURE' F41.3 // )
      WRITE(3,205) SIG,CF,T,D,L
  205 FORMAT(' '31X'LINER PARAMETERS'//
     110X'CAVITY OPEN AREA RATIO'F48.4/
     210X'FLOW COEFFICIENT'F54.3/
     310X'APERTURE LENGTH (IN)'F50.3/
     410X'APERTURE DIAMETER (IN)'F48.3/
     510X'CAVITY BACKING DEPTH (IN)'F45.3)
      WRITE(3,206) XLEFF,APARE,XK2
  206 FORMAT(10X'EFFECTIVE APERTURE LENGTH (IN)'F40.3/
     110X'APERTURE AREA (IN**2)'F49.4/
     210X'RESISTANCE COEFFICIENT' F48.3 // )
      RRFO = KO*KO*APARE/144./PI2
      B= XK2/CF2
      PIPP =2.* B*P1/GAMA
      MO = SQRT(RRFO*RRFO/4.+PIPP) -RRFO/2.
      UORFO = MO*SONIC/B
      RESFO = MO
      MO = MO/B
      IF (MT-MO/2.) 22,21,21
   21 RESFO = MT/CF**3
      GO TO 23
   22 IF(MP*SONIC/UORFO*(TEMPC/TEMP)**2  -1.5) 23,23,24
   24 RESFO = B*MP/3.*(TEMPC/TEMP)**2 +MO/2.*B
   23 BETAO = RESFO/RRFO
      EPSLO =4.*BETAO /(BETAO+1.)**2
      QUALO=SONIC*XLEFF*12.0/APARE/(BETAO+1.0)/FO
      PI = P1*PRESS/SQRT(2.)
      PID =20.*.4343*ALOG(PI/29.E-10)
      PIP=PI*SQRT(2.)
      ENABO=.5*DEN*APARE/144.*(SONIC*MO)**3*B/G
      WRITE(3,207) PID,PIP,UORFO,RESFO,RRFO
  207 FORMAT(' '20X'LINER ACOUSTIC PARAMETERS AT RESONANCE'//
     110X'RMS AMPLITUDE OF INCIDENT PRESSURE (DECIBELS)' F25.2 /
     210X'PEAK AMPLITUDE OF INCIDENT PRESSURE (PSIA)'    F28.5 /
     310X'ORIFICE VELOCITY AT RESONANCE (FT/SEC)'F32.1/
     410X'DISSIPATION RESISTANCE (DIMENSIONLESS)'        F32.3 /
     510X'RADIATION RESISTANCE (DIMENSIONLESS)'          F34.3 )
      WRITE(3,208) BETAO,EPSLO,QUALO,ENABO,FO
  208 FORMAT(10X'RESISTANCE RATIO, DISSIPATION-TO-RADIATION'F28.3/
     110X'RESONATOR COEFFICIENT AT RESONANCE'F36.3/
     210X'QUALITY FACTOR'F56.3/
     310X'ENERGY ABSORBED (FT*LBF/SEC)'E42.4/
```

```
     410X'RESONANT FREQUENY (HZ)'F48.1  )
      FREQ=FMIN
    7 WRITE (3,6)
    6 FORMAT (1H1)
      WRITE (3,200) TITLE
  200 FORMAT (    1X,20A4,//)
      LINE = 1
      WRITE (3,209)
  209 FORMAT(11X'FREQ'4X'RFREQ'4X'REACT'6X'RESIS'4X'RADRX'3X'UORFX'3X
     1'BETAX'3X'RCOEF'4X'POWAB'6X'CRITA' / )
  603 CONTINUE
      RFREQ=FREQ/FO
      CRITA=D*FREQ/L/SONIC/3.
      RADRX = RRFO*RFREQ**2
      KOL=KO*L/12.
      KL=KOL*RFREQ
      KT=KO*RFREQ*XLEFF/12.
      REACT=(SIG*COS(KL)/SIN(KL)-SIN(KT)/COS(KT))
      X=MO*B
      DELA=X/4.0
      CALL SOLVM (FUNKU,YACT,X,TOL,DELA,YCAL)
      UORFX = X*SONIC/B
      RESIS = X
      IF (MT-UORFX/SONIC/2.) 25,26,26
   26 RESIS = MT/CF**3
      GO TO 27
   25 TR= (TEMPC / TEMP) **2
      IF( MP*SONIC/UORFX*TR- 1.5) 27,27,28
   28 RESIS= B*MP/3.*TR+ X/2.
   27 BETAX = RESIS / RADRX
      RCOEF = 4.0*BETAX/((BETAX + 1.0)**2 + (REACT/RADRX)**2)
      ENABX=ENABO*RESIS/RESFO*(UORFX/UORFO)**2
      WRITE (3,211) FREQ,RFREQ,REACT,RESIS,RADRX,UORFX,BETAX,RCOEF,ENABX
     1,CRITA
      LINE = LINE + 1
  211 FORMAT( F16.1, F8.3,2F10.4,F9.4, F8.2,2F8.3,2E12.4)
      IF(FREQ-FMAX) 601,602,602
  601 FREQ=FREQ+DELF
      IF (LINE-50) 603,7,7
  602 IF (P1 - SPLM) 401, 406, 406
  401 P1=P1+DELP
      GO TO 303
  406 CONTINUE
      CALL EXIT
      END
// XEQ
```

5. Output For Sample Cases

EXAMPLE CASE, NO FLOW

GAS PROPERTIES

STATIC PRESSURE (PSIA)	60.000
APERTURE GAS TEMP (DEG. R)	3000.0
GAS CONSTANT (LBF*FT/LBM/R)	45.700
RATIO OF SPECIFIC HEATS	1.200
GAS DENSITY (LBM/FT**3)	0.0630
GAS SONIC VELOCITY(FT/SEC)	2300.6
COMBUSTION GAS TEMP (DEG R)	6000.0
MACH NO OF FLOW PAST APERTURE	0.000
MACH NO OF FLOW THRU APERTURE	0.000

LINER PARAMETERS

CAVITY OPEN AREA RATIO	0.6131
FLOW COEFFICIENT	1.000
APERTURE LENGTH (IN)	0.075
APERTURE DIAMETER (IN)	0.730
CAVITY BACKING DEPTH (IN)	0.636
EFFECTIVE APERTURE LENGTH (IN)	0.350
APERTURE AREA (IN**2)	0.4185
RESISTANCE COEFFICIENT	0.370

LINER ACOUSTIC PARAMETERS AT RESONANCE

RMS AMPLITUDE OF INCIDENT PRESSURE (DECIBELS)	177.28
PEAK AMPLITUDE OF INCIDENT PRESSURE (PSIA)	2.99999
ORIFICE VELOCITY AT RESONANCE (FT/SEC)	771.9
DISSIPATION RESISTANCE (DIMENSIONLESS)	0.124
RADIATION RESISTANCE (DIMENSIONLESS)	0.124
RESISTANCE RATIO, DISSIPATION-TO-RADIATION	0.999
RESONATOR COEFFICIENT AT RESONANCE	1.000
QUALITY FACTOR	1.927
ENERGY ABSORBED (FT*LBF/SEC)	0.4844E 03
RESONANT FREQUENY (HZ)	6000.4

EXAMPLE CASE, NO FLOW

FREQ	RFREQ	REACT	RESIS	RADRX	UORFX	BETAX	RCOEF	POWAB	CRITA
5000.0	0.833	0.2723	0.0943	0.0862	586.65	1.093	0.304	0.2126E 03	0.8315E 00
5100.0	0.849	0.2429	0.1000	0.0897	621.97	1.114	0.377	0.2534E 03	0.8481E 00
5200.0	0.866	0.2141	0.1055	0.0932	656.13	1.131	0.461	0.2975E 03	0.8647E 00
5300.0	0.883	0.1859	0.1106	0.0969	688.16	1.141	0.552	0.3432E 03	0.8813E 00
5400.0	0.899	0.1581	0.1152	0.1006	716.72	1.145	0.647	0.3877E 03	0.8980E 00
5500.0	0.916	0.1308	0.1191	0.1043	740.65	1.141	0.741	0.4279E 03	0.9146E 00
5600.0	0.933	0.1039	0.1220	0.1082	759.18	1.128	0.827	0.4608E 03	0.9312E 00
5700.0	0.949	0.0773	0.1240	0.1120	771.53	1.106	0.900	0.4837E 03	0.9479E 00
5800.0	0.966	0.0512	0.1250	0.1160	777.70	1.077	0.955	0.4954E 03	0.9645E 00
5900.0	0.983	0.0254	0.1250	0.1201	777.70	1.041	0.988	0.4954E 03	0.9811E 00
6000.0	0.999	-0.0000	0.1241	0.1242	771.91	0.999	1.000	0.4844E 03	0.9978E 00
6100.0	1.016	-0.0252	0.1223	0.1283	760.91	0.953	0.989	0.4640E 03	0.1014E 01
6200.0	1.033	-0.0502	0.1197	0.1326	744.90	0.903	0.959	0.4353E 03	0.1031E 01
6300.0	1.049	-0.0749	0.1166	0.1369	725.21	0.851	0.913	0.4017E 03	0.1047E 01
6400.0	1.066	-0.0994	0.1129	0.1413	702.44	0.799	0.856	0.3650E 03	0.1064E 01
6500.0	1.083	-0.1236	0.1089	0.1457	677.35	0.747	0.792	0.3273E 03	0.1080E 01
6600.0	1.099	-0.1477	0.1046	0.1502	650.72	0.696	0.724	0.2902E 03	0.1097E 01
6700.0	1.116	-0.1716	0.1002	0.1548	623.32	0.647	0.656	0.2550E 03	0.1114E 01
6800.0	1.133	-0.1954	0.0959	0.1595	596.30	0.601	0.591	0.2233E 03	0.1130E 01
6900.0	1.149	-0.2190	0.0915	0.1642	569.29	0.557	0.530	0.1943E 03	0.1147E 01
7000.0	1.166	-0.2424	0.0873	0.1690	543.43	0.516	0.474	0.1690E 03	0.1164E 01

EXAMPLE CASE, PAST FLOW

GAS PROPERTIES

STATIC PRESSURE (PSIA)	60.000
APERTURE GAS TEMP (DEG. R)	3000.0
GAS CONSTANT (LBF*FT/LBM/R)	45.700
RATIO OF SPECIFIC HEATS	1.200
GAS DENSITY (LBM/FT**3)	0.0630
GAS SONIC VELOCITY(FT/SEC)	2300.6
COMBUSTION GAS TEMP (DEG R)	6000.0
MACH NO OF FLOW PAST APERTURE	0.150
MACH NO OF FLOW THRU APERTURE	0.000

LINER PARAMETERS

CAVITY OPEN AREA RATIO	0.6131
FLOW COEFFICIENT	1.000
APERTURE LENGTH (IN)	0.245
APERTURE DIAMETER (IN)	0.730
CAVITY BACKING DEPTH (IN)	0.636
EFFECTIVE APERTURE LENGTH (IN)	0.350
APERTURE AREA (IN**2)	0.4185
RESISTANCE COEFFICIENT	0.370

LINER ACOUSTIC PARAMETERS AT RESONANCE

RMS AMPLITUDE OF INCIDENT PRESSURE (DECIBELS)	177.28
PEAK AMPLITUDE OF INCIDENT PRESSURE (PSIA)	2.99999
ORIFICE VELOCITY AT RESONANCE (FT/SEC)	771.6
DISSIPATION RESISTANCE (DIMENSIONLESS)	0.136
RADIATION RESISTANCE (DIMENSIONLESS)	0.124
RESISTANCE RATIO, DISSIPATION-TO-RADIATION	1.093
RESONATOR COEFFICIENT AT RESONANCE	0.997
QUALITY FACTOR	1.837
ENERGY ABSORBED (FT*LBF/SEC)	0.4839E 03
RESONANT FREQUENY (HZ)	6003.7

EXAMPLE CASE, PAST FLOW

FREQ	RFREQ	REACT	RESIS	RADRX	UORFX	BETAX	RCOEF	POWAB	CRITA
5000.0	0.832	0.2728	0.1211	0.0862	586.24	1.404	0.355	0.2487E 03	0.8315E 00
5100.0	0.849	0.2435	0.1239	0.0897	621.16	1.381	0.423	0.2856E 03	0.8481E 00
5200.0	0.866	0.2147	0.1267	0.0932	655.50	1.358	0.500	0.3252E 03	0.8647E 00
5300.0	0.882	0.1864	0.1292	0.0969	687.52	1.333	0.583	0.3650E 03	0.8813E 00
5400.0	0.899	0.1587	0.1315	0.1006	715.68	1.307	0.669	0.4025E 03	0.8980E 00
5500.0	0.916	0.1314	0.1335	0.1043	739.99	1.279	0.754	0.4367E 03	0.9146E 00
5600.0	0.932	0.1045	0.1349	0.1082	758.51	1.247	0.833	0.4639E 03	0.9312E 00
5700.0	0.949	0.0780	0.1360	0.1120	771.24	1.213	0.901	0.4833E 03	0.9479E 00
5800.0	0.966	0.0518	0.1365	0.1160	777.41	1.176	0.953	0.4928E 03	0.9645E 00
5900.0	0.982	0.0260	0.1365	0.1201	777.41	1.136	0.985	0.4928E 03	0.9811E 00
6000.0	0.999	0.0006	0.1360	0.1242	771.82	1.095	0.997	0.4842E 03	0.9978E 00
6100.0	1.016	-0.0245	0.1351	0.1283	761.02	1.053	0.990	0.4677E 03	0.1014E 01
6200.0	1.032	-0.0495	0.1339	0.1326	745.39	1.009	0.966	0.4445E 03	0.1031E 01
6300.0	1.049	-0.0742	0.1323	0.1369	725.33	0.966	0.929	0.4158E 03	0.1047E 01
6400.0	1.065	-0.0986	0.1305	0.1413	702.95	0.923	0.882	0.3853E 03	0.1064E 01
6500.0	1.082	-0.1229	0.1285	0.1457	677.87	0.881	0.829	0.3527E 03	0.1080E 01
6600.0	1.099	-0.1469	0.1263	0.1502	651.44	0.840	0.774	0.3204E 03	0.1097E 01
6700.0	1.115	-0.1708	0.1241	0.1548	624.24	0.801	0.718	0.2891E 03	0.1114E 01
6800.0	1.132	-0.1945	0.1220	0.1595	597.04	0.764	0.664	0.2598E 03	0.1130E 01
6900.0	1.149	-0.2181	0.1198	0.1642	570.23	0.729	0.613	0.2328E 03	0.1147E 01
7000.0	1.165	-0.2416	0.1177	0.1690	543.99	0.696	0.566	0.2081E 03	0.1164E 01

*END

APPENDIX D
REFERENCES

1. Ingard, Uno, "On the Theory and Design of Acoustic Resonators," JASA, Vol. 25, No. 6, November 1953, p 1037.

2. "Suppression of Combustion Oscillations with Mechanical Damping Devices, Interim Report," Pratt & Whitney Aircraft, PWA FR-3299, 8 August 1969.

3. Ingard, Uno and H. Ising, "Acoustic Nonlinearity of an Orifice," JASA, Vol. 42, No. 1, July 1967.

4. Kinsler, T. E. and A. R. Frey, Fundamentals of Acoustics, Second Edition, John Wiley and Sons, Inc., New York.

5. "Suppression of Combustion Oscillations with Mechanical Damping Devices, Phase II Interim Report," Pratt & Whitney Aircraft, PWA FR-3880, 26 June 1970.

6. Phillips, B., "Recent Advances in Acoustic Liner Technology at Lewis Research Center," 5th ICRPG Combustion Conference CPIA Pub No. 183, December 1968.

7. Garrison, G. D., et al., "Acoustic Liner Design and Demonstration Final Report," Pratt & Whitney Aircraft Technical Report AFRPL-TR-71-71, August 1971.

8. "A Study of the Suppression of Combustion Oscillations with Mechanical Damping Devices Final Report," Pratt & Whitney Aircraft, PWA FR-2596, November 1967.

9. Sabine, W. C., Collected Papers on Acoustics, Harvard University Press, Cambridge, Massachusetts, 1922.

10. "Sound Absorption of Acoustical Materials in Reverberation Rooms," ASTM Report C 423-60T, 1960.

11. Young, R. W., "Sabine Reverberation Equation and Sound Power Calculations," JASA, Vol. 31, No. 7, p 921, July 1959.

12. Knudsen, V. O., "Effect of Humidity Upon the Absorption of Sound in a Room, and a Determination of the Coefficients of Absorption of Sound in Air," JASA, Vol. 3, p 126, 1931.

REFERENCES (Continued)

13. Parkinson, J. S., "Area and Pattern Effects in the Measurement of Sound Absorption," JASA, Vol. 2, No. 1, pp 112-122, July 1930.

14. Chresler, V. L., Discussion, JASA, Vol. 11, p 97, 1939.

15. Tyzzer, F. G. and H. A. Leedy, "Advances Since 1929 in Methods of Testing Acoustical Performance of Acoustical Materials," JASA, Vol. 26, No. 5, p 655, September 1954.

16. Dolansky, L. O., "Studio for Listening Tests," JASA, Vol. 30, No. 3, p 175, March 1958.

17. Bedell, E. H. and K. D. Swartzel, "Reverberation Time and Absorption Measurements with the High Speed Level Recorders," JASA, Vol. 6, p 130, January 1935.

18. Schultz, T. J., "Problems in the Measurement of Reverberation Time," Journal of the Audio Engineering Society, Vol. 11, No. 4, p 307, October 1963.

DISTRIBUTION LIST

Copies	Recipient	Designee
	NASA Headquarters Washington, D.C. 20546	
1	Contracting Officer	X
	NASA-Lewis Research Center 21000 Brookpark Road Cleveland, Ohio 44135	
1	Office of Technical Information	X
	NASA-Manned Spacecraft Center Houston, Texas 77001	
1	Office of Technical Information	X
	NASA-Marshall Space Flight Center Marshall Space Flight Center, Alabama 35812	
2	Office of Technical Information, MS-IP	X
1	Technical Library	X
1	Dale Burrows, S&E-ASTN-PJ	X
1	Robert Richmond, S&E-ASTN-PP	X
1	Rex Bailey, S&E-ASTN-PPB	X
2	Richard Counts, S&E-ASTN-PPB	X
	Jet Propulsion Laboratory 4800 Oak Grove Drive Pasadena, California 91103	
2	Louis Toth	X
3	Chief, Liquid Propulsion Technology, RPL Office of Advanced Research and Technology NASA Headquarters Washington, D. C. 20546	X
1	Director, Technology Utilization Division Office of Technology Utilization NASA Headquarters Washington, D. C. 20546	X
20	NASA Scientific and Technical Information Facility P. O. Box 33 College Park, Maryland 20740	X
1	Director, Launch Vehicles and Propulsion, SV Office of Space Science and Applications NASA Headquarters Washington, D. C. 20546	X
1	Director, Advanced Manned Missions, MT Office of Manned Space Flight NASA Headquarters Washington, D. C. 20546	X

DISTRIBUTION LIST (Continued)

Copies	Recipient	Designee
	NASA Pasadena Office 4800 Oak Grove Drive Pasadena, California 91103	
1	Patents and Contracts Management	X
	Western Support Office 150 Pico Boulevard Santa Monica, California 90406	
1	Office of Technical Information	X
	Jet Propulsion Laboratory 4800 Oak Grove Drive Pasadena, California 91103	
1	D. D. Lawson, Technical Monitor	X
	Rocket Research Laboratories Edwards Air Force Base Edwards, California 93253	
1	Technical Librarian	X
1	Lt. Wayne Pritz, RPRRG	X
	NASA FIELD CENTERS	
1	Ames Research Center Moffett Field, California 94035	Hans M. Mark
1	Goddard Space Flight Center Greenbelt, Maryland 20771	Merland L. Moseson Code 620
2	Jet Propulsion Laboratory California Institute of Technology 4800 Oak Grove Drive Pasadena, California 91103	Henry Burlage, Jr. Propulsion Div. 38
1	Langley Research Center Langley Station Hampton, Virginia 23365	Ed Cortwright Director
1	Lewis Research Center 21000 Brookpark Road Cleveland, Ohio 44135	Director
1	Manned Spacecraft Center Houston, Texas 77001	J. G. Thibodaux, Jr. Chief, Prop. and Power Div

DISTRIBUTION LIST (Continued)

Copies	Recipient	Designee
1	John F. Kennedy Space Center, NASA Cocoa Beach, Florida 32931	Dr. Kurt H. Debus
	GOVERNMENT INSTALLATIONS	
1	Air Force Missile Test Center Patrick Air Force Base, Florida	L. J. Ullian
1	Space and Missile Systems Organization Air Force Unit Post Office Los Angeles, California 90045	Colonel Clark Technical Data Center
1	Arnold Engineering Development Center Arnold Air Force Station Tullahoma, Tennessee 37388	Dr. H. K. Doetsch
1	Bureau of Naval Weapons Department of the Navy Washington, D. C. 20546	J. Kay RTMS-41
1	Defense Documentation Center Headquarters Cameron Station, Building 5 5010 Duke Street Alexandria, Virginia 22314 Attn: TISIA	
1	Headquarters, U. S. Air Force Washington, D. C. 20546	Colonel C. K. Stambaugh AFRST
1	Picatinny Arsenal Dover, New Jersey 07801	T. Forsten, Chief Liquid Propulsion Laboratory
1	Air Force Rocket Propulsion Laboratory Research and Technology Division Air Force Systems Command Edwards, California 93523	RPRPD/Mr. H. Main
1	U. S. Army Missile Command Redstone Arsenal, Alabama 35809	Dr. Walter Wharton
1	U. S. Naval Ordnance Test Station China Lake, California 93557	CODE 4562 Chief, Missile Propulsion Div.
1	Aeronautical Systems Division Air Force Systems Command Wright-Patterson Air Force Base Dayton, Ohio 45433	D. L. Schmidt Code ASRCNC-2

DISTRIBUTION LIST (Continued)

Copies	Recipient	Designee
1	Air Force Missile Development Center Holloman Air Force Base New Mexico 88330	Maj. R. E. Bracken
	CPIA	
1	Chemical Propulsion Information Agency Applied Physics Laboratory 8621 Georgia Avenue Silver Spring, Maryland 20910	Tom Reedy
	INDUSTRY CONTRACTORS	
1	Aerojet-General Corporation P. O. Box 296 Azusa, California 91703	W. L. Rogers
1	Aerojet-General Corporation P. O. Box 1947 Technical Library, Bldg. 2015, Dept. 2410 Sacramento, California 95809	R. Stiff
1	Space Division Aerojet-General Corporation 9200 East Flair Drive El Monte, California 91734	S. Machlawski
1	Aerospace Corporation 2400 E. El Segundo Boulevard P. O. Box 95085 Los Angeles, California 90045	John G. Wilder MS-2293
1	Atlantic Research Company Edsall Road & Shirley Highway Alexandria, Virginia 22314	Dr. Ray Friedman
1	Avco Systems Division Wilmington, Massachusetts	Howard B. Winkler
1	Beech Aircraft Corporation Boulder Division Box 631 Boulder, Colorado	J. H. Rodgers
1	Bell Aerosystems Company P. O. Box 1 Buffalo, New York 14240	W. M. Smith

DISTRIBUTION LIST (Continued)

Copies	Recipient	Designee
1	Bellcomm 955 L'Enfant Plaza, S. W. Washington, D. C.	H. S. London
1	Boeing Company P. O. Box 3707 Seattle, Washington 98124	J. D. Alexander W. W. Kann
1	Boeing Company 1625 K. Street, N. W. Washington, D. C. 20006	Library
1	Missile Division Chrysler Corporation P. O. Box 2628 Detroit, Michigan 48231	John Gates
1	Wright-Aeronautical Division Curtis-Wright Corporation Woodridge, New Jersey 07075	G. Kelley
1	Research Center Fairchild Hiller Corporation Germantown, Maryland	Ralph Hall
1	General Dynamics, Convair Division Library & Information Services (128-00) P. O. Box 1128 San Diego, California 92112	Frank Dore
1	Missile and Space Systems Center General Electric Company Valley Forge Space Technology Center P. O. Box 8555 Philadelphia, Pennsylvania	F. Mezger F. E. Schultz
1	Grumman Aircraft Engineering Corporation Bethpage, Long Island, New York 11714	Joseph Gavin
1	Honeywell, Inc. Aerospace Division 2600 Ridgway Road Minneapolis, Minnesota	Gordon Harms
1	Hughes Aircraft Company Aerospace Group Centinela and Teale Streets Culver City, California 90230	F. H. Meter V. P. and Div. Mgr.

DISTRIBUTION LIST (Continued)

Copies	Recipient	Designee
1	Walter Kidde and Company, Inc. Aerospace Operations 567 Main Street Belleville, New Jersey	R. J. Hanville Dir. of Research Engr.
1	Ling-Temco-Vought Corporation P. O. Box 5907 Dallas, Texas 75222	Warren G. Trent
1	Arthur D. Little, Inc. 20 Acorn Park Cambridge, Massachusetts 02140	Library
1	Lockheed Missiles and Space Company Attn: Technical Information Center P. O. Box 504 Sunnyvale, California 94088	J. Guill
1	Lockheed Propulsion Company P. O. Box 111 Redlands, California 92374	Library
1	The Marquardt Corporation 16555 Saticoy Street Van Nuys, California 91409	Library
1	Baltimore Division Martin Marietta Corporation Baltimore, Maryland 21203	John Calathes (3214)
1	Denver Division Martin Marietta Corporation P. O. Box 179 Denver, Colorado 80201	Dr. Morgenthaler A. J. Kullas
1	Astropower Laboratory McDonnell Douglas Astronautics Company 2121 Bloomfield Avenue Newport Beach, California 92663	Dr. George Moe
1	Astrosystems International, Inc. 1275 Bloomfield Avenue Fairfield, New Jersey 07007	A. Mendenhall
1	Missile and Space Systems Division McDonnell Douglas Astronautics Company 3000 Ocean Park Boulevard Santa Monica, California 90406	Mr. R. W. Hallet Chief Engineer Adv. Space Tech.

DISTRIBUTION LIST (Continued)

Copies	Recipient	Designee
1	Space & Information Systems Division North American Rockwell 12214 Lakewood Boulevard Downey, California 90241	Library
1	Rocketdyne (Library 586-306) 6633 Canoga Avenue Canoga Park, California 91304	Dr. R. J. Thompson J. A. Nestlerode
1	Northrop Space Laboratories 3401 West Broadway Hawthorne, California 90250	Dr. William Howard
1	Aeronutronic Division Philco Corporation Ford Road Newport Beach, California 92663	D. A. Garrison
1	Rocket Research Corporation 520 South Portland Street Seattle, Washington 98108	Foy McCullough, Jr.
1	Stanford Research Institute 333 Ravenswood Avenue Menlo Park, California 94025	Dr. Gerald Marksmen
1	TRW Systems Group TRW Incorporated One Space Park Redondo Beach, California 90278	G. W. Elverum
1	Thiokol Chemical Corporation Aerospace Services Elkton Division Bristol, Pennsylvania	Library
1	Research Laboratories United Aircraft Corporation 400 Main Street East Hartford, Connecticut 06108	Erle Martin
1	Hamilton Standard Division United Aircraft Corporation Windsor Locks, Connecticut 06096	R. Hatch
1	United Technology Center 587 Methilda Avenue P. O. Box 358 Sunnyvale, California 94088	Dr. David Altman

DISTRIBUTION LIST (Continued)

Copies	Recipient	Designee
1	Space General Corporation 9200 East Flair Avenue El Monte, California 91734	C. E. Roth
1	Thiokol Chemical Corporation Huntsville Division Huntsville, Alabama	John Goodloe
	Princeton University Forrestal Research Center Princeton, New Jersey 08540	
1	Dr. I. Glassman	
	Princeton University Forrestal Research Center Princeton, New Jersey 08540	
1	Mr. D. T. Harrje	
	University of Wisconsin Dept. of Mechanical Engineering 1513 University Avenue Madison, Wisconsin 53705	
1	Dr. P. S. Myers	
	Dartmouth University Hanover, New Hampshire	
1	Dr. P. D. McCormack	
	University of Michigan Aeronautical & Astronautical Engineering Laboratories Aircraft Propulsion Lab. North Campus Ann Arbor, Michigan	
1	Dr. J. A. Nicholls	
	Institute of Engineering Research University of California Berkeley, California	
1	Dr. A. K. Oppenheim	
	Purdue University School of Mechanical Engineering Lafayette, Indiana	
	Dr. J. R. Osborn	

DISTRIBUTION LIST (Continued)

Copies	Recipient	Designee
	Massachusetts Institute of Technology Department of Mechanical Engineering Cambridge, Massachusetts 02139	
1	Dr. T. Y. Toong	
	Illinois Institute of Technology 10 W. 35th Street Chicago, Illinois	
1	Dr. P. T. Torda	
	The Pennsylvania State University Mechanical Engineering Department 207 Mechanical Eng. Boulevard University Park, Pennsylvania 16802	
1	G. M. Faeth	
	Georgia Institute of Technology Aerospace School Atlanta, Georgia 30332	
1	Dr. B. T. Zinn Dr. J. M. Delhaye	
	Polytechnic Institute of Brooklyn Graduate Center Route 110	
1	Farmingdale, New York	Dr. V. D. Agosta
	Applied Physics Laboratory The Johns Hopkins University 8621 Georgia Avenue	
1	Silver Spring, Maryland 20910	Dr. W. G. Berl
1	Ohio State University Rocket Research Laboratory Department of Aeronautical & Astronautical Engineering Columus, Ohio 43201	